AIChE

Fundamentals-Based Low-Dimensional Combustion Modeling of Spark-Ignited Internal Combustion Engines

Pankaj Kumar
Dept. of Chemical and Biomolecular Engineering, University of Houston, Houston, TX 77204

Matthew Franchek and Karolos Grigoriadis
Dept. of Mechanical Engineering, University of Houston, Houston, TX 77204

Vemuri Balakotaiah
Dept. of Chemical and Biomolecular Engineering, University of Houston, Houston, TX 77204

DOI 10.1002/aic.12447
Published online November 15, 2010 in Wiley Online Library (wileyonlinelibrary.com).

A four-mode low-dimensional model for the in-cylinder combustion process in an internal combustion engine is developed. The lumped parameter ordinary differential equation model is based on two mixing times that capture the reactant mixing limitations inside the cylinder and mixing limitations caused by the input and exit stream distribution. For a given inlet and operating conditions, the model predicts the exhaust composition of regulated gases (total unburned HCs, CO, and NO_x) as well as the in-cylinder pressure and temperature. The model is able to capture the qualitative trends observed with change in fuel composition (gasoline and ethanol blending), air/fuel ratio, spark timing, engine load, and speed. The results show good qualitative and fair quantitative agreement with the experimental results published in the literature and demonstrate the possibility of such low-dimensional model for real-time control. Improvements and extensions to the model are discussed. © 2010 American Institute of Chemical Engineers *AIChE J*, 57: 2472–2492, 2011
Keywords: combustion, mathematical modeling, mixing, reactor analysis, reaction kinetics

Introduction

The current trend toward simultaneously increasing fuel-to-wheels efficiency while reducing emissions from transportation system powertrains requires system level optimization realized through real-time multivariable control. Such an optimization can be accomplished using low-order fundamentals (first-principles)-based models for each of the engine sub systems, i.e., in-cylinder combustion processes, exhaust after-treatment systems, mechanical and electrical systems (for hybrid vehicles), and sensor and control systems. The combustion process and catalytic after-treatment systems can be described by the fundamental conservation laws (species, momentum, and energy) of diffusion-convection-reaction type. Such a description consisting of many partial differential equations with coupling between the transport process and the complex chemistry is extremely demanding computationally and has limited utility for system level optimization studies. For online optimization and real-time control, these physics-based models must be low-dimensional, retain the qualitative features of the system, and have sufficient quantitative accuracy. In our view, the bottleneck for attaining real-time onboard system

Correspondence concerning this article should be addressed to V. Balakotaiah at bala@uh.edu.

level optimization is the lack of accurate low-dimensional models for the internal combustion (IC) engine.

Several models have been developed in the literature to simulate the spark ignition engine cycle.[1–3] These can be broadly categorized as fluid dynamic models or thermodynamic models, depending on whether the governing equation is derived from the detailed fluid flow or by considering the thermodynamics laws. The fluid dynamics-based models are also popularly termed as "multi-dimensional models," as they can give the detailed solution including the spatial variations inside the cylinder. Here, the governing equations are obtained by using the species, momentum, and energy balances resulting in partial differential equations in time and space which makes these models computationally very demanding (in terms of memory and speed).

Thermodynamic models are developed using the first law of thermodynamics together with mass balance.[1,4] As spatial variation is not considered in these models, they form a set of ODEs in time only and are thus also called zero-dimensional models. The most commonly used thermodynamic model is the "two-zone" model, where the complete cylinder is treated as a single zone for the entire engine cycle other than combustion during which it is divided into two zones known as burned and unburned zones separated by a thin ignition film. Before combustion, all the mass is assumed to be unreacted as unburned zone and after combustion the whole mass is treated as burned zone, with two separate zones during combustion. To model the combustion part, usually two different approaches are used. In the first method, a predefined empirical mass burning relations like the cosine burn rate or the Wiebe function is used.[1] These relations require combustion start time and combustion duration to be provided as input. As these properties depend strongly on the engine operating conditions (such as air/fuel ratio and fuel composition), the method has limitations in terms of extension to different operating regimes. In the second approach, combustion is modeled using a turbulent flame propagation model.[1] However, ignition of the cylinder charge is not modeled, rather start of combustion is initialized by assuming instantaneous formation of ignition kernel at or shortly after the ignition timing.[3] Also, the flame propagation speed, which is determined empirically, will be a function of operating conditions.

The "zero-dimensional" model lacks the effect of spatial variation, whereas the multidimensional fluid dynamic model is computationally very expensive. In this work, we develop a low-dimensional model for IC engine cycle by using a spatially averaged three-dimensional detailed convection-diffusion-reaction (CDR) model.[5] The derived model includes the relevant physics and chemistry occurring at different time and length scales but is in the form of a few ordinary differential equations so that it can be used for parametric studies and real-time optimization and control. The combustion of gasoline is modeled by using the global reaction kinetics. Thus, the model does not require prespecification of combustion time, as it can automatically predict ignition caused by the rise in temperature after the spark discharge. The model also predicts the composition of the exhaust gases and the effect of various design and operating variables on the exhaust gas composition.

We describe the low-dimensional model in some detail in the next section. The model is used to predict the influence of various operating variables on the exhaust gas composition and the in-cylinder temperature and pressure. The predictions are compared to available experimental data in the literature. We also discuss briefly some possible extensions or further improvements to the model and how it may be integrated with exhaust after-treatment models.

Model Development

The spark ignition (SI) engine cycle consists of four consecutive steps: intake, compression, power (combustion and expansion), and exhaust. It is an open system with time dependent control volume (function of crank angle). The instantaneous volume of the cylinder $V(t)$ as a function of crank angle is given by,[1]

$$\frac{V(t)}{V_c} = 1 + \frac{1}{2}(r_c - 1)\left[\widehat{R} + (1 - (\cos\theta(t))) - \left(\widehat{R}^2 - \left(\sin^2\theta(t)\right)\right)^{1/2}\right], \quad (1)$$

where, V_c is the clearance volume, r_c is the compression ratio, $\widehat{R}$ is the ratio of connecting rod length to crank radius, and $\theta(t)$ is the crank angle at any time t.

Differentiating Eq. 1 w.r.t. time we get,

$$\frac{dV}{dt} = V_c\left(\frac{1}{2}(r_c - 1)\left[\sin\theta + \frac{\sin\theta\cos\theta}{\left(\widehat{R}^2 - \sin^2\theta\right)^{1/2}}\right]\right)\Omega,$$

where, $\Omega = \frac{d\theta}{dt}$ is the angular speed. In this work, Ω is kept constant. The combustion in SI engine is initiated by spark discharge which in turn raises the temperature around the spark plug which ignites the gases leading to the flame front propagation. This phenomenon of gas combustion can best be analyzed by considering the reaction kinetics instead of using empirical mass burn relations. However, the detailed chemical kinetics for gasoline combustion will involve more than 500 different intermediate species with thousands of reactions as shown by Curran et al.[6] Hence, the global reaction kinetics is used, which has been shown to be able to capture the relevant trends quite accurately.[7–9] Gasoline is a complex chemical mixture of several hundred hydrocarbons. For simplicity, we represent gasoline as composed of 80% fast burning hydrocarbon and 20% slow burning. As shown later, this two lump representation is the simplest that can predict properly the exit unburned hydrocarbon as well as temperature maxima for slightly richer condition. The peak temperature occurs at around stoichiometry for one lump, while it shifts to a richer side with two lumps which agrees with the trend reported in literature for gasoline combustion.[1] Next to model the combustion process, the simplest approach will be to model combustion cylinder as an ideal (perfectly mixed) single compartment with uniform concentration and temperature throughout the cylinder. Although this simplest model may predict the fuel blending and stoichiometric effects (such as the NO_x maximum at slightly leaner conditions) as well as the in-cylinder temperature and pressure with reasonable accuracy, it gives errors in predicting hydrocarbon conversion as it omits the importance of crevice effect which is considered as one of the major reason for unburned hydrocarbon emissions.[1] As shown later, the ideal model also predicts higher in-cylinder temperature and hence higher NO_x concentration. Thus, the next simplest model includes the crevice effect, the large difference in the temperature of the in-cylinder gases and the outer wall of the cylinder, and the mixing effects within the cylinder due to flow field and molecular or turbulent diffusion. In this work, we focus on this next simplest non-trivial model and assume that the combustion chamber can be modeled as comprised of two control volumes where the cylinder contents exchange species and energy with relatively very small volume of the crevice (aggregated as single block of constant volume) whose temperature can be taken as the same as the wall temperature. Further, we do not assume infinitely fast mixing in the combustion chamber but introduce two mixing times that account for the effect of finite mixing between reactants and products. Our model reduces to the ideal combustion chamber model in the limit of these mixing times approaching zero. The model formulation is discussed below.

Species balance

We extend the recently developed two-mode species balance model by Bhattacharya et al.[5] for constant volume system, to model the variable volume IC engine combustion chamber. We refer to Appendix A for details and explain here only the main concepts. The combustion cylinder is divided into N number of smaller compartments interacting with each other [Remark: The number N could be arbitrarily large but in practice, it is sufficient to use four to six compartments]. The detailed convection-diffusion-reaction (CDR) model is used for each compartment followed by Lyapunov-Schmidt (LS) technique to develop a low-dimensional model in two modes using the cup-mixing (or flow weighted) concentration C_m and the volume averaged concentration $\langle C \rangle$. As discussed in Appendix A and in more detail elsewhere,[5] in the limit of both mixing times vanishing, the spatial gradients become negligible, and the model reduces to the classical ideal or perfectly mixed (CSTR) model. When the mixing times are small but finite, the LS procedure retains the same accuracy and relevant qualitative features as the detailed CDR model.[5] The important point to note is that the conversion of the reactants (fuel) is determined by the flow weighted concentration C_m, whereas the reaction (combustion) rates are evaluated at the volume averaged concentration $\langle C \rangle$. The volume averaged species balance equation in the two-mode form is given by

$$\frac{d(\langle C_j \rangle)}{dt} = \frac{1}{V}\left[F_j^{\mathrm{in}} - F_j + \sum_{i=1}^{N_{\mathrm{R}}} v_{ij} R_i(\langle C \rangle)V - \langle C_j \rangle \frac{dV}{dt} - F_{j,\mathrm{cr}}\right] \tag{2}$$

$$\frac{d(C_{cr,j})}{dt} = \frac{1}{V_{\mathrm{cr}}}\left[F_{j,\mathrm{cr}} + \sum_{i=1}^{N_{\mathrm{R}}} v_{ij} R_i(C_{\mathrm{cr}})V_{\mathrm{cr}}\right], \tag{3}$$

$$C_{m,j} - \langle C_j \rangle = t_{\mathrm{mix},2} C_{m,j}^{in} - t_{\mathrm{mix},1} C_{m,j}, \tag{4}$$

$$F_{j,cr} = Q_{cr}(aC_{m,j} - (1-a)C_{cr_j}), \tag{5}$$

where the suffix i and j stands for the reaction number and the gaseous component, respectively. Here, N_{R} is the total number of reactions, $C_{m,j}$ and $\langle C_j \rangle$ are the flow (velocity) weighted concentration and volume averaged concentration of the jth component, respectively. F_j^{in} and F_j (=QC_{m}) are the molar flow rates in and out of the cylinder, respectively. v_{ij} gives the stoichiometric coefficient defined in standard notation as negative for reactants and positive for products. $R_i(\langle C \rangle)$ is the rate of the ith reaction evaluated at the volume averaged concentrations and in-cylinder temperature. Similarly, $R_i(C_{\mathrm{cr}})$ represents rate of reaction evaluated at crevice concentration and wall temperature condition. Equations 2 and 3 gives the overall species balance for the jth component within the cylinder and inside the crevice region, respectively. The species balance accounts for the change in species concentration within the cylinder due to mass flow in and out, generation by chemical reaction, volume change and crevice flow effect. Equation 4 represents the interaction between two averaged concentrations $C_{m,j}$ and $\langle C_j \rangle$, expressed in terms of dimensionless mixing times $t_{\mathrm{mix},1}$ and $t_{\mathrm{mix},2}$ which accounts for the non uniformity in the cylinder. The time $t_{\mathrm{mix},1}$ depends on the diffusivities of the reactant species, engine speed, swirl ratio, and the velocity gradients in the cylinder, i.e., it captures the mixing limitations inside the cylinder. The mixing time $t_{\mathrm{mix},2}$ accounts for the feed distribution (premixed or unmixed) effect as well as the mixing between the feed and the products. The dependence of feed stream distribution like number of valves, flow through each valve etc. is captured by the inlet cup mixing concentration ($C_{m,j}^{\mathrm{in}}$). As discussed in more detail in Appendix A, if the feed (air and fuel) is premixed and there is no overlap between intake valve and exhaust valve timing, the dimensionless time $t_{\mathrm{mix},2}$ becomes zero. The parameter $t_{\mathrm{mix},1}$, being a function of intake and exhaust flow will be function of time; however, for simplicity in this work, we assume a cycle averaged value for mixing time ($t_{\mathrm{mix},1} = 0.2$).

In Eq. 5, Q_{cr} and C_{cr} are the exchange flow rate (between the main flow and the crevice) and the concentration in the crevice region, respectively. The crevice is modeled as an isolated zone within the cylinder with a total volume (V_{cr}) equal to 3.5% of the clearance volume and characterized by very high surface/volume ratio such that its temperature can be assumed to be same as the cylinder wall temperature. [Since the crevice volume is small, no distinction is made between the cup-mixing and volume averaged concentrations in the crevice]. The parameter "a" in Eq. 5 determines the direction of flow. When the in-cylinder pressure is higher than the crevice pressure, the flow is into the crevice ($a = 1$) and when the flow is out of crevice and into the cylinder $a = 0$. The rate of flow into or out of crevice is modeled using flow through a valve given by

$$Q_{\mathrm{cr}} = Q_{\mathrm{cr},0}\sqrt{|P - P_{\mathrm{crevice}}|}, \tag{6}$$

where $Q_{\mathrm{cr},0}$ is the function of crevice area and flow drag coefficient. The average pressure inside the combustion cylinder and the pressure within the crevice region are given by P and P_{crevice}, respectively, which are obtained using an ideal gas law as

$$P = \left(\sum_{j=1}^{N_c} C_{m,j}\right) RT, \tag{7}$$

and

$$P_{\text{crevice}} = \left(\sum_{j=1}^{N_c} C_{\text{cr},j}\right) RT_{\text{wall}}. \quad (8)$$

In the above expressions, $R = 8.314$ J/K mol is the universal gas constant and N_c is total number of gaseous components. The total inlet volumetric flow rate is the cumulative sum of the air ($Q_{\text{in}}^{\text{air}}$) and fuel flow rates ($Q_{\text{in}}^{\text{fuel}}$). The air flow rate can be computed using first principles based air path dynamic model[10] as follows

$$Q_{\text{in}}^{\text{air}} = \eta_{\text{vol}} \frac{V_{\text{d}}}{2} \frac{\Omega}{2\pi}. \quad (9)$$

Here, V_{d} is the engine displacement ($V_{\text{d}} = (r_{\text{c}} - 1)V_{\text{c}}$). The volumetric efficiency η_{vol} of the induction process is given by

$$\eta_{\text{vol}} = E\frac{\gamma - 1}{\gamma} + \frac{r_{\text{c}} - \left(\dfrac{P_{\text{amb}}}{P_{\text{man}}}\right)}{\gamma(r_{\text{c}} - 1)}, \quad (10)$$

where E is an experimentally determined quantity, γ is specific heat ratio, P_{amb} and P_{man} are the ambient and inlet manifold pressures, respectively. The inlet concentration of air can be computed using ideal gas law at ambient temperature and manifold pressure condition. For a given air intake throttle position i.e. for a constant air flow-rate, the amount of fuel to be injected should decrease with increase in blending (for example, x_{e}, the mole fraction of ethanol in the fuel) as well as for increase in desired λ $\left(\frac{\text{air/fuel}}{(\text{air/fuel})_s}\right)$. Thus for a given air flow, the required fuel flow rate to obtain normalized air/fuel ratio of λ can be computed as

$$Q_{\text{in}}^{\text{fuel}} = \frac{1}{\lambda(10.6 - 7.6x_{\text{e}})} Q_{\text{in}}^{\text{air}}. \quad (11)$$

The numerical factors 10.6 and 7.6 follow from the stoichiometry of fuel combustion with oxygen. For example, as 1 mole of ethanol reacts with 3 moles of O_2 for complete combustion, we see from Eq. 11, that for pure ethanol ($x_{\text{e}} = 1$) at stoichiometry ($\lambda = 1$), the molar flow rate of air is 3 times the molar flow rate of fuel. Similarly, for 1 mole of iso-octane (C_8H_{18}), 12.5 mole of oxygen is required and for C_2H_4, 3 moles of O_2 is required. Thus, for 80–20% fast and slow burn representation of gasoline considered, we need molar air flow rate that is 10.6 times that of molar fuel flow rate to obtain $\lambda = 1$. Next, the concentration of gases entering the cylinder can be calculated using ideal gas law at manifold pressure and ambient temperature condition and choosing mole fraction to satisfy λ requirement.

The exit volumetric flow rate is modeled as the flow through an orifice and is expressed as

$$Q = C_{\text{d}} A_{th} \sqrt{2(P - P_{\text{out}})/\rho}, \quad (12)$$

where C_{d} is a drag coefficient, A^{th} is the exhaust valve area, P is the cylinder pressure, P_{out} is the downstream pressure (assumed constant), and ρ is the instantaneous density of gaseous mixture inside combustion chamber. No backflow of gases from exit manifold to the cylinder was allowed and thus for the duration when the exhaust valve is open the flow is either out given by Eq. 12 or is zero. The above assumption will not be valid for valve overlap case and will be considered in future work. The combustion reactions are highly exothermic, so there exists a huge variation in the temperature during a single combustion cycle. In the following section, we formulate the energy balance equation to capture the thermal effects.

Energy balance

The First Law of Thermodynamics for an open system is given by

$$\dot{Q}_{\text{heat}} - \dot{W}_{\text{s}} + \sum_{j=1}^{N_c} F_j^{in} H_j^{in} - \sum_{j=1}^{N_c} F_j H_j = \frac{\partial \hat{E}}{\partial t}, \quad (13)$$

where $\dot{Q}_{\text{heat}}$ is the net rate of flow of heat to the system, $\dot{W}_{\text{s}}$ is the rate of shaft work (which includes the work done by piston movement) done by the system on the surrounding, H_j^{in} and H_j are the molar enthalpies of the jth gaseous component at cylinder inlet and exit conditions, respectively. Here, $\hat{E}$ is the total internal energy of the system. Equation 13 along with the species balance Eq. 2 can be simplified to obtain the energy balance equation as

$$\begin{aligned}\frac{dT}{dt} = {} & \frac{1}{\left(\sum_{j=1}^{Nc} \langle C_j \rangle V (C_{p_j} - R)\right)} \\ & \times \Bigg[\dot{Q}_{\text{spark}} - \dot{Q}_{\text{coolant}} - P\dot{V} + \sum_{j=1}^{N_c} F_j^{\text{in}} (H_j^{\text{in}} - H_{\ j}) \\ & + RT \sum_{j=1}^{N_c} \frac{d(\langle C_j \rangle V)}{dt} + \sum_{i=1}^{N_{\text{R}}} R_i(\langle C \rangle) V \left(-\triangle H_{R,i}\right)_T \\ & + Q_{\text{cr}}(1-a) \sum_{j=1}^{N_c} C_{\text{cr}j} \left(H_j^{\text{cr}} - H_j\right) \Bigg]. \quad (14)\end{aligned}$$

A detailed derivation of energy balance Eq. 14 is shown in Appendix B. In the above equation, $\dot{Q}_{\text{spark}}$ is the rate of energy added by the spark and is modeled as an external energy source[11] that adds sufficient energy to ignite the system. $\dot{Q}_{\text{coolant}}$ is the heat transferred from the bulk gas to the wall and $(\Delta H_{R,i})_T$ gives the heat of ith reaction at temperature T [Remark: For exothermic reactions, $(-\Delta H_{R,i})$ is positive]. C_{p_j} is the specific heat of gas at constant pressure. Equilibrium constant, heat of reaction, and specific heat are all computed using thermodynamic laws and are evaluated as functions of temperature. The thermodynamic properties are taken from standard textbook.[12] Equations 2 and 14 describe the general species and energy balance that are valid for the entire cycle of the IC engine. However, depending upon the stage of IC engine cycle, the different terms entering the species and energy balance equations need to be properly assigned. For example, the inlet flow rate will be nonzero only during the intake stroke. The physical properties of the gases used in Eq. 14 are calculated assuming ideal gas behavior. The term containing $\dot{Q}_{\text{coolant}}$ in Eq. 14 is determined using a pseudo steady state assumption as explained in the next section.

Heat transfer

Heat is transferred from gases inside the combustion cylinder to chamber wall by convection and radiation and through the chamber wall by conduction. In addition, there is convection from outside the cylinder wall. For a steady one-dimensional heat flow through a wall, the following equations relate the heat flux $\left(\dot{q} = \dot{Q}_{\text{coolant}}/A\right)$ and the temperatures.

Heat transfer from the bulk gas to cylinder wall is given by,

$$\dot{q}_{\text{g}} = h_{\text{c,g}}\left(T - T_{\text{w,g}}\right) + \sigma\varepsilon\left(T^4 - T^4_{\text{w,g}}\right), \tag{15}$$

where $h_{\text{c,g}}$ is gas side heat transfer coefficient which is computed using Woschni's correlation,[1] T and $T_{\text{w,g}}$ are the average bulk gas temperature and gas side wall temperature respectively, ε is the emissivity, and σ is the Stefan -Boltzman constant [$5.67 \times 10^{-8} W/(m^2K^4)$]. Heat transfer within the cylinder wall is given as,

$$\dot{q}_{\text{w}} = \frac{k\left(T_{\text{w,g}} - T_{\text{w,c}}\right)}{l}, \tag{16}$$

where $T_{w,c}$ is the coolant side wall temperature, l is the wall thickness, and k is the thermal conductivity of wall, assumed constant. Heat transfer from the cylinder wall to the engine coolant is given as,

$$\dot{q}_{\text{c}} = h_{\text{c,c}}\left(T_{\text{w,c}} - T_{\text{c}}\right), \tag{17}$$

where $h_{\text{c,c}}$ is coolant heat transfer coefficient and T_{c} is coolant temperature. Both $h_{\text{c,c}}$ and T_{c} are assumed constant. Assuming pseudo steady state ($\dot{q}_{\text{g}} = \dot{q}_{\text{w}} = \dot{q}_{\text{c}} = \dot{q}$), Eqs. 15–17 can be solved to obtain wall heat flux ($\dot{q}$). However as Eq. 15 is non linear, we use an iterative method. First an initial guess for heat flux ($\dot{q}$ is obtained by neglecting the radiation as shown in Eq. 18

$$\dot{q} = \frac{(T - T_{\text{c}})}{\left(\frac{1}{h_{\text{c,g}}} + \frac{l}{k} + \frac{1}{h_{\text{c,g}}}\right)}. \tag{18}$$

This initial guess for heat flux is used to compute gas side wall temperature ($T_{\text{w,g}}$) by solving Eqs. 16 and 17. And thus finally using that wall temperature, the actual heat flux is computed using Eq. 15 and thus computing a non linear equation by solving linear equations iteratively.

To compute the convective heat transfer coefficient on the gas side, Woschni's correlation[1] is used:

$$h_{\text{c,g}} = 3.26 B^{-0.2} p^{0.8} T^{-0.55} w^{0.8}. \tag{19}$$

Here, B is cylinder bore, p is the instantaneous cylinder pressure measured in KPa, and w is the average cylinder gas velocity given by

$$w = C_1 S_p + C_2 \frac{V_d T_r}{p_r V_r}(p - p_m), \tag{20}$$

where p_{r}, V_{r}, and T_{r} are reference pressure, temperature, and volume, respectively. In this work, the reference value were chosen to be the condition during closing of intake valve. S_{p} is the mean piston speed given by $S_{\text{p}} = 2LN$, where L ($= (r_{\text{c}} - 1)l_{\text{c}}$) is the stroke length and N is the engine speed. p_{m} is the motored pressure at the same crank angle as p. The motored pressure is the pressure that would have been achieved in the absense of combustion, due to piston movement alone. It can be computed assuming adiabatic expansion with cylinder pressure to equilibrate with inlet pressure at bottom dead center ($V = r_{\text{c}}V_{\text{c}}$).

Table 1. Woschni's Correlation Parameters[1]

Engine Cycle Period	C_1	C_2 $(mK^{-1}s^{-1})$
Gas exchange period	6.18	0
Compression period	2.28	0
Combustion and expansion period	2.28	3.24×10^{-3}

$$p_{\text{m}} = \left(\frac{r_{\text{c}}V_{\text{c}}}{V}\right)^{\gamma} p_{\text{in}}. \tag{21}$$

The constants C_1 and C_2 for Eq. 20 are given in Table 1.

Fuel composition and global reaction kinetics models

As stated earlier, gasoline is a complex mixture of over 500 different hydrocarbons that have between 5 to 12 carbon atoms. To represent gasoline combustion properly, one would need to use lumped species model to correctly include the characteristic combustion behavior of all the major contributing groups involved. For example, if four lumps are to be used then species from aliphatic, straight chain, branched and cyclic compounds and aromatic compound can be included. Also if blended fuel is used, ethanol should also be included as another lump to represent the fuel composition. For simplicity, in this work, we use a two-lump model comprising of fast burn and a slow burning hydrocarbon group to model gasoline. The fast burn component is one that oxidizes earlier in a mixture containing the two components. In this work, reaction 1 as shown in Table 2 is fast burn, whereas reaction 2 corresponds to slow burn.

Gasoline is usually represented by $CH_{1.875}$; however, no single chemical species has carbon and hydrogen composition in that proportion. It is also well known that iso-octane (C_8H_{18}) exhibits property similar to gasoline and thus the choice component for major group. However, the H:C ratio in iso-octane is 2.25 so as to bring the H:C ratio lower we use $(CH_2)_n$ which has H:C ratio of 2 and also is one of the known intermediate of gasoline combustion. The ideal choice for slow burning component could be CH_4; however, because of its very high H:C ratio, we represent the slow component by $(CH_2)_2$, whose kinetics was modified to have rate of combustion slower than iso-octane combustion.

It was observed that a two lump model for gasoline is the simplest that can correctly predict phenomena such as peak temperature attaining maximum for slightly richer condition. This preliminary two lump model can easily be extended to multiple lumps, and this will be considered in future work.

Similar to the fuel composition complexity, the combustion reaction kinetics can also be very complicated. The detailed chemical kinetics for hydrocarbon combustion

Table 2. Global Kinetic Rate Constant used for Gasoline-Ethanol Combustion (in SI units)

No	Reaction	A	β	E_a	Orders of Reaction	ref
1	$C_8H_{18} + \frac{17}{2}O_2 \rightarrow 3CO + 4H_2O$	1.8×10^{22}	0	1.25×10^5	$[C_8H_{18}]^{0.25}[O_2]^{1.5}$	Westbrook[7]
2	$(CH_2)_n + nO_2 \rightarrow nCO + nH_2O$	6.01×10^{22}	0	1.25×10^5	$[(CH_2)_n]^{0.1}[O_2]^{1.85}$	(modified)
3f	$CO + \frac{1}{2}O_2 \rightarrow CO_2$	1.26×10^{25}	0	1.67×10^5	$[CO][H_2O]^{0.5}[O_2]^{0.25}$	Westbrook[7]
3b	$CO_2 \rightarrow CO + \frac{1}{2}O_2$	5×10^{14}	0	1.67×10^5	$[CO_2]$	Westbrook[7]
4f	$CO + H_2O \rightarrow CO_2 + H_2$	2.75×10^{24}	0	8.36×10^4	$[CO][H_2O]$	Jones[8]
4b	$CO_2 + H_2 \rightarrow CO + H_2O$		0		$[CO_2][H_2]$	
5f	$N_2 + O_2 \rightarrow 2NO$	6×10^{25}	−0.5	5.74×10^5	$[O_2]^{0.5}[N_2]$	Heywood[1]
5b	$2NO \rightarrow N_2 + O_2$		−0.5		$[NO]^2[O_2]^{-0.5}$	
6	$H_2 + \frac{1}{2}O_2 \rightarrow H_2O$	1.8×10^{22}	0	1.44×10^5	$[H_2][O_2]^{0.5}$	Marinov[9]
7	$C_2H_5OH + 2O_2 \rightarrow 2CO + 3H_2O$	5.7×10^{22}	0	1.25×10^5	$[C_2H_5OH]^{0.15}[O_2]^{1.6}$	Westbrook[7]

involves more than 500 different intermediate species with thousands of reactions,[7] but they are not suitable for low-dimensional modeling. Global kinetics becomes critical in that case as they can describe the system behavior with relatively fewer equations, in terms of final species only. The global reaction schemes shown in Table 2 were considered for the work.

All the reaction rates in Table 2 are expressed as

$$r_i = A_i T^{\beta_i} \exp\left(-\frac{E_{a_i}}{RT}\right) \prod_{j=1}^{N_c} [C_j]^{n_j}, \tag{22}$$

where r_i is rate of reaction expressed in mol/(m^3.s). The frequency factor A_i, temperature exponent β_i, activation energy E_{a_i} are listed in columns 2, 3, and 4 of Table 2, respectively, whereas column 5 gives the orders of the reaction with respect to various species involved, corresponding to terms $\prod_{j=1}^{N_c}[C_j]^{n_j}$ in Eq. 22. For reversible reactions, the reverse rate constants for the N_2 oxidation and water-gas shift reactions vary with temperature and are computed using equilibrium relations.

In the simplified scheme considered in this work, reactions 1, 2, and 7 represent the partial combustion of fuel. Reaction 3 is further oxidation of CO to CO_2. Reaction 4 is known as water-gas shift reaction and is the major path for production of H_2 in combustion. Reaction 5 is representative of NO_x formation, whereas reaction 7 is ethanol combustion that occurs for ethanol blended gasoline fuel. Finally, reaction 6 represents the combustion of hydrogen produced by the water-gas shift reaction. [Remark: We note that the NO formation and water-gas shift reactions in Table 2 satisfy the thermodynamic constraints but not the CO oxidation. This is due to the fact that CO is considered as an intermediate combustion product in the global kinetic scheme and the kinetics of CO oxidation in Table 2 was obtained in conjunction with HC oxidation.]

Before presenting the simulation results, we consider briefly the manifold dynamics. Shown in Figure 1 is the variation of manifold pressure with change in throttle plate angle at constant rpm. The first principle model commonly used in the literature[10] is used to simulate intake manifold dynamics. As the throttle angle is increased, the air intake flow cross-sectional area increases. This increases the intake air flow rate and thus the manifold pressure goes up. As can be observed from Figure 1, the manifold pressure attains steady state very quickly. Thus, a pseudo steady state assumption was applied, and the intake manifold pressure was assumed constant at 0.8 atm in further computations using the low-dimensional combustion model.

The low-dimensional model for combustion as described above consists of ordinary differential equations(ODEs) representing the various species balances and the energy balance equation. For the two-lump gasoline blends considered in this work, the model equations consists of 10 species (or $N_c = 10$) (C_8H_{18}, $(CH_2)_2$, O_2, CO_2, H_2O, N_2, CO, NO, H_2, C_2H_5OH) balances each for the crevice and combustion cylinder (Eqs. 2 and 3) and an energy balance equation (Eq. 14) making total of 21 ODEs [Note: Since the cup-mixing and volume averaged concentrations in the combustion chamber are related linearly through the algebraic relation, Eq. 4, the former is not counted as unknown]. It is assumed that the feed (air) enters the intake manifold at ambient conditions, atmospheric pressure, and 298 K. The cylinder temperature is also initialized to the ambient value, and thus, the first few cycles in the simulations shown in Figure 2 represents the cold start of the engine and then the system attains a periodic steady state. It should be pointed out that the set of ODEs are highly stiff and hence require standard stiff-ODE solvers, which are readily available in MATLAB or FORTRAN (such as ODE15s, ODE23s etc. in MATLAB or LSODE in FORTRAN).

The model equations contain several design parameters and operating variables. As our goal here is to validate the model by comparing the model predictions with available

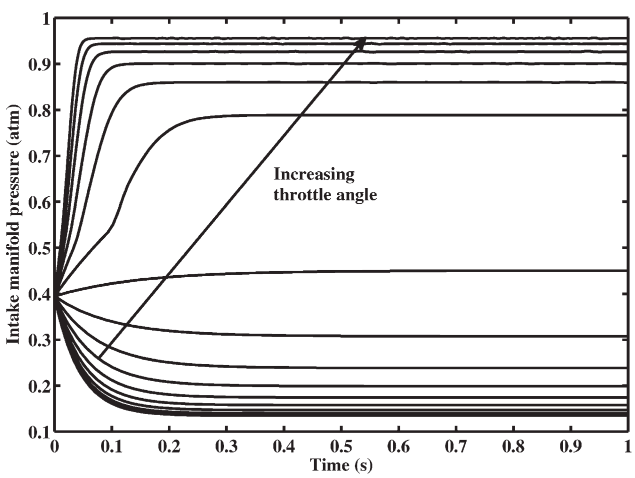

Figure 1. Intake manifold pressure variation with throttle position as a function of time.

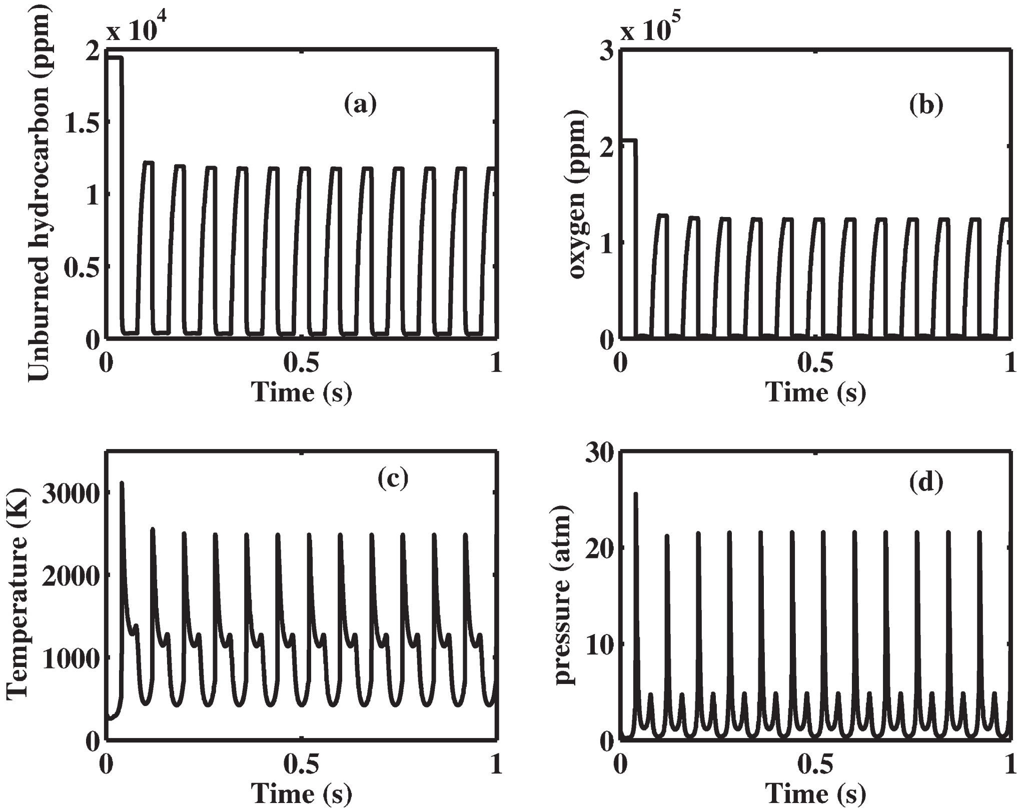

Figure 2. In-cylinder temporal variation of (a) total unburned hydrocarbon concentration, (b) unburned oxygen concentration, (c) in-cylinder temperature, and (d) in-cylinder Pressure.

experimental data and examine some key trends (and not an exhaustive parametric study), we have fixed the values of some of these parameters as shown in Table 3.

Simulation of IC Engine Behavior and Emissions Using the Low-Dimensional Model

Shown in Figures 2 and 3 are the variation of the combustion products concentrations, the temperature and pressure inside the combustion chamber under stoichiometric ($\lambda = 1$) conditions, as predicted by the low-dimensional combustion model. The following observations follow from these plots: (i) as expected, the IC engine attains a periodic steady-state very quickly (within fraction of a second) even from a cold-start condition. (ii) The unburned hydrocarbon concentration (Figure 2a) rises during intake and compression stage, reaching its maximum value just before the combustion and then drops sharply after the ignition. There exists a corresponding peak in temperature and pressure caused by the heat released by the highly exothermic combustion reactions. These sharp gradients in temperature, pressure, and concentrations are the reason for the stiffness of the model. (iii) From Figure 3, we can also conclude that among all currently regulated gas emissions considered here, the NO_x emission is most sensitive to temperature, especially to the peak temperature (as can be expected). Although all other emissions attains fairly steady state value after just the first cycle, the NO_x emission shows most noticeable change before its value is stabilized after around 4–5 cycles, which is the same amount of time as taken by the temperature to achieve its steady state value.

Shown in Figure 4 is the temporal variation of pressure and temperature in the cylinder over a single cycle, after a periodic steady-state is attained. The complete cycle comprises of two revolution or 4π crank angle rotation. At $\theta = 0^0$, the intake valve opens and the the premixed air–fuel

Table 3. System Parameters

System Parameters	Value
Bore diameter, B	7.67×10^{-2} m
Clearance length, l_c	1.27×10^{-2} m
rpm	1500
Compression ratio, r_c	9
Crank length/Rod, $\hat{R}$	4
Cylinder wall thickness, l	1×10^{-2} m
Coolant thermal conductivity, $h_{c,c}$	750 W/m^{2}K
Wall thermal conductivity, k	54 W/mK
Ambient temperature	298 K
Ambient pressure, P_{amb}	1.01×10^5 Pa
Exhaust manifold pressure, P_{out}	1.115×10^5 Pa
Inlet manifold pressure, P_{man}	0.81×10^5 Pa
Coolant temperature, T_c	373 K
C_d	0.1
E	0.6
γ	1.33
$t_{mix,1}$	0.2
$t_{mix,2}$	0

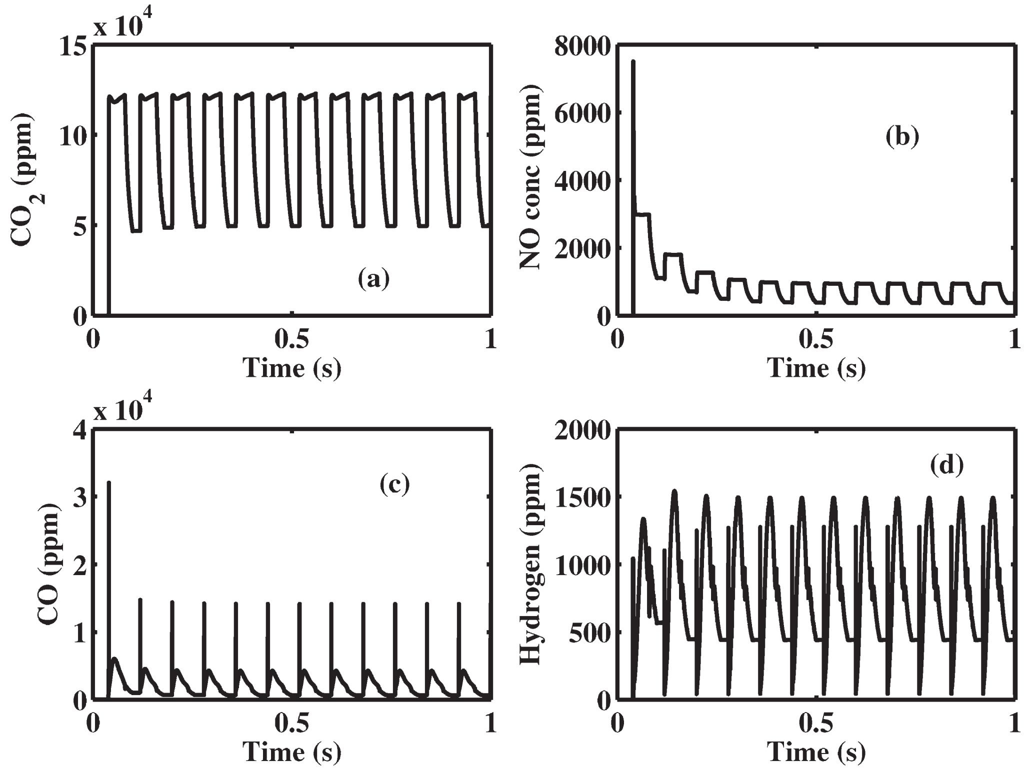

Figure 3. Temporal variation of in-cylinder (a) CO_2 concentration, (b) NO_x concentration, (c) CO concentration and (d) hydrogen concentration.

mixture enters the system. The feed gases (air charge) are at lower temperature (298K) compared to the gases left in the cylinder after the previous combustion cycle, thus we see a dip in temperature initially. Similarly, for the pressure during the intake stroke, the volume is increasing and so is the number of moles of gases in the cylinder. Thus, from Figure 4, it appears that initially the volume increase dominates the moles added and there is a drop in pressure but eventually a pseudo steady state is reached and pressure is almost constant during the intake stroke. From $\theta = 180^0$, when the piston reaches the bottom dead center (BDC), the compression stroke begins. Because of the compression work done by the piston, we see an increase in temperature and pressure. In Figure 4, the crank angle of 12^0 to 8.5^0 before top dead center (BTDC) represent the time period during which spark was activated. Then, after a small delay, combustion starts leading to a sharp rise in the temperature and pressure. The model predicts a smaller delay after ignition when compared with a real system, because unlike the present model where whole mass ignites at once, in a real system ignition occurs through flame front propagation introducing a delay to obtain peak temperature. This phenomenon can be captured by using a multi compartment type low–dimensional model and will be considered in future work. It can be observed that the rise in temperature due to combustion is much higher when compared with the temperature or pressure rise due to energy provided by the spark. For the power stroke, we see a drop in pressure and temperature as the cylinder volume increases. After $\theta = 540^0$, the exhaust valves are opened and the gases are expelled out.

Shown in Figure 5 is the concentrations of various exhaust gases coming out of the combustion chamber. As the exhaust valve opens periodically, we see pulses of exhaust gas

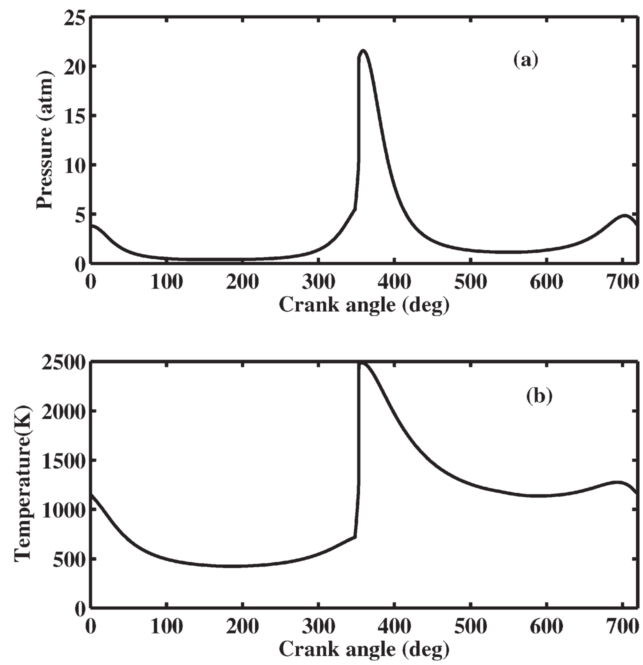

Figure 4. In-cylinder variation of (a) pressure and (b) temperature during a complete cycle after a periodic state is attained.

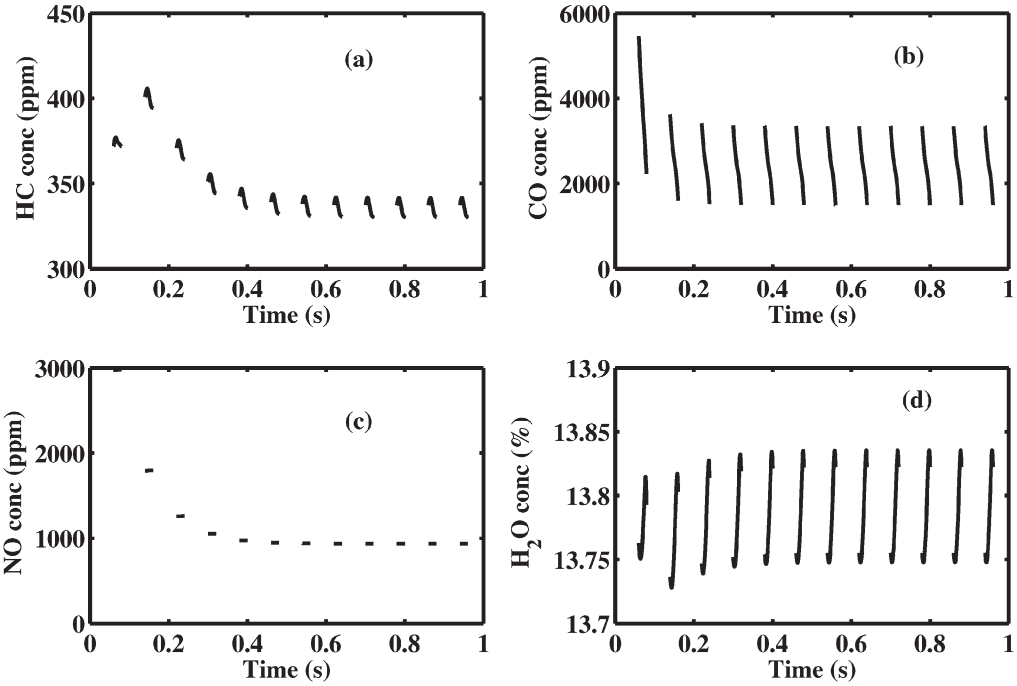

Figure 5. Variation of exhaust gas concentrations with time (a) unburned hydrocarbon, (b) CO emission, (c) exhaust NO_x, and (d) Exhaust H_2O.

concentration at exit. Although the reaction is almost over by the time exhaust valve opens, we still observe change in concentration at the exit, because of the change in volume of the reactor and also because of moles exiting the reactor. As shown in Figure 5, the model predicts an average NO_x concentration of around 920 ppm, CO around 0.3%, unburned hydrocarbon around 320 ppm, and around 13.8% water in the exhaust. These numbers agree qualitatively with results presented in the Ref. 13, where the relative ranges of exhaust concentrations suggested are: NO_x 100–3000 ppm and unburned hydrocarbons (HC) 500–1000 ppm. The unburned hydrocarbon predicted is on the lower side because we do not include conversion of gasoline to intermediate hydrocarbons and also because of absence of valve overlap in this model, which contributes to a significant amount of unburned hydrocarbon. Also, the CO prediction is lower than the experimentally reported value of around 1–2%, as the H:C ratio in the fuel considered is higher than that observed in gasoline ($\simeq 1.875$). The CO prediction decreased when the fuel was changed from octane to propane, which has relatively lower C:H ratio. Results with different fuel composition are discussed in the work of Kumar.[14] A second possible reason may be that the CO oxidation kinetics used in this study was obtained under fuel lean condition and may need to be modified to accommodate the fuel rich condition. Shown in Figure 6 is the normalized reaction rates as a function of temperature during a single cycle. The rate of oxidation of fast burning hydrocarbon, CO and N_2 are shown in Figure 6a. As expected, the CO oxidation reaction starts after the hydrocarbon is oxidized to CO. Around the peak temperature (T = 2500 K), the HC rate is almost zero, implying that most of the reactants are converted by the time the peak temperature is reached. It can be observed from the plot that the NO_x formation requires very high temperature and reaches a maximum value when the system temperature is maximum. The reaction rate for water gas shift reaction (WGS) and hydrogen oxidation shows similar trend because of coupling of CO and H_2 through the WGS reaction. When WGS is high, more H_2 will be produced leading to higher reaction rate for H_2 oxidation and vice versa. Shown in Figure 7 is conversion as a function of crank angle over a cycle. The fast burn hydrocarbon goes to almost a complete conversion. And because of the presence of slow burning hydrocarbon, the total conversion is around 97% w.r.t. total hydrocarbon. The burn duration ($x_b = 0$ to $x_b \approx 1$) as predicted by the model is around 45^0 which is in close agreement with the values reported in Ref. 1. This supports our assumption that the global kinetic models used are sufficient to represent the detailed complex combustion mechanism for predicting the regulated gas emissions. Unlike the Wiebe function–based model where burn duration and ignition delay are predefined parameter, the major advantage of using kinetics to represent combustion is that these parameters are computed automatically based on species reactivity and system temperature.

Effect of air to fuel ratio

We now use the low-dimensional model to study the effect of air to fuel ratio (λ) on the exhaust gas composition. Shown in Figure 8 is the variation of peak temperature and pressure with change in λ. The peak temperature occurs for slightly richer condition which is in agreement with the trends observed in Ref. 1. The two peaks observed corresponds to the fast and slow burning component, respectively. It was observed that with one lump for gasoline, the peak temperature occurred around stoichiometry. And the peak

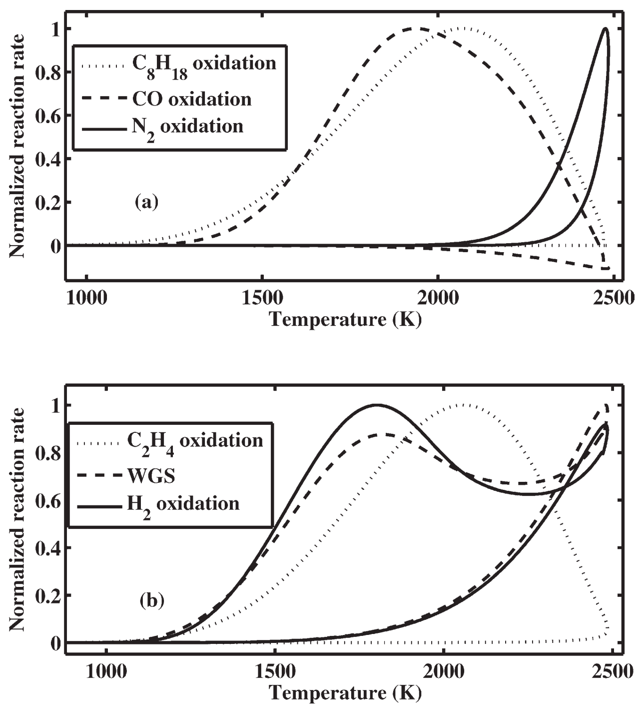

Figure 6. Normalized reaction rates as a function of temperature over a cycle.

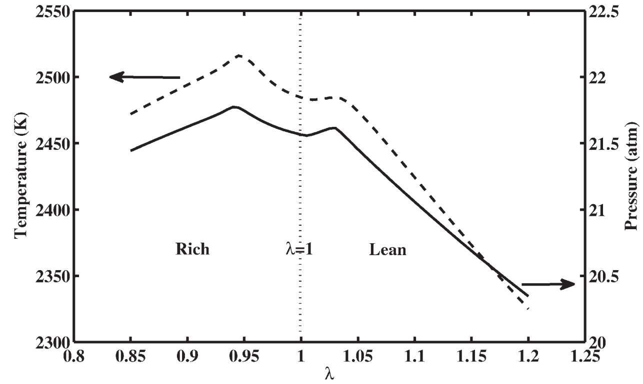

Figure 8. Effect of change in air/fuel ratio on peak temperature and pressure.

temperature will shift toward the richer side with increase of slow burning component. This happens because although the overall λ may be rich, it becomes close to stoichiometry just w.r.t. fast burn component, which can react with oxygen first because of higher reactivity, thereby showing the maxima. Shown in Figure 9 is the variation of average mole fractions (ppm) of exhaust gases with change in air-fuel ratio at constant rpm =1500 and the throttle plate position (constant inlet pressure). The flow rate of air and fuel was kept constant at the same value as stoichiometry, only the composition (mole fraction) of inlet feed was manipulated to change λ_{in}. We can observe that leaner mixture gives lower emissions in terms of unburned hydrocarbon and carbon monoxide. However, if we make the mixture too lean, the combustion quality becomes poorer and eventually misfire will occur. As expected, for the rich operating conditions CO and HC emissions rise sharply. The NO_x concentration shows a maxima w.r.t. air to fuel ratio λ. This is observed because NO_x formation is a strong function of temperature and oxygen concentration (nitrogen is always in excess). From the reaction rate vs. temperature Figure 6, it is obvious that the NO formation starts after the HC oxidation. Thus, at very rich conditions, not enough oxygen is present to oxidize (or react with) the nitrogen, while at very lean condition, the temperature is low for the NO formation reaction to occur. The peak temperature occurs at slight rich condition (Figure 8), however there is not enough oxygen present then for NO formation. Thus, as the mixture is leaned out, the initial decrease in temperature is offset by the increase in oxygen concentration, and the peak for NO concentration is observed at slightly leaner condition, around $\lambda = 1.05$. These model predicted results agree qualitatively with those reported in the Ref. 1,13.

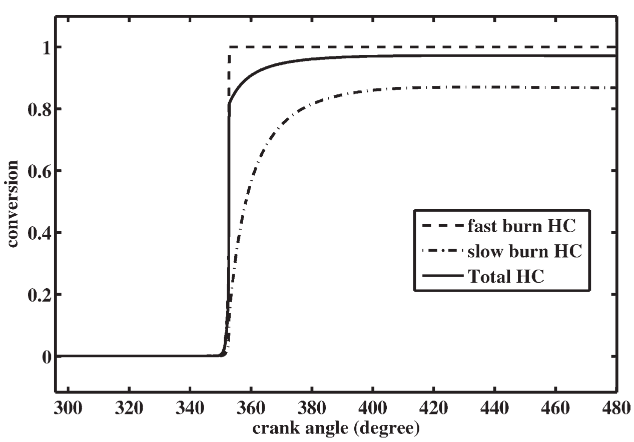

Figure 7. Hydrocarbon conversion with crank angle for $\lambda = 1$.

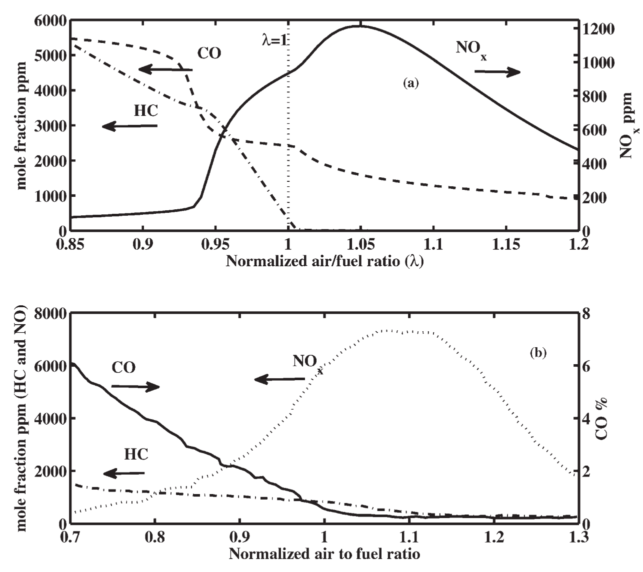

Figure 9. Variation of regulated exhaust gases with air fuel ratio (a) predicted from low-dimensional model and (b) experimentally observed.[13]

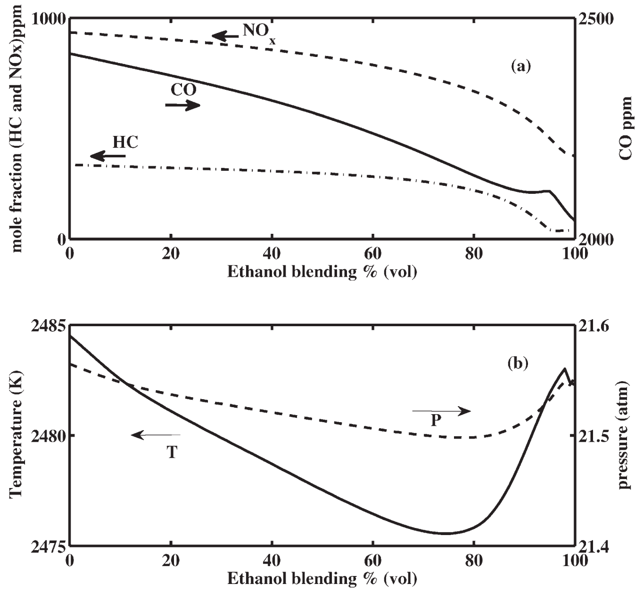

Figure 10. (a) Impact of blending on emissions and (b) in-cylinder temperature and pressure under constant normalized air/fuel ratio of λ = 1.

Effect of fuel blending

It is well known that the CO and HC concentration decreases with the ethanol blending. However, for NO_x emissions, there is a slight ambiguity as some work in the literature[15,16] has shown NO_x to be increasing with blending, while other works[17,18] presents a decreasing trend. The difference arises from whether the normalized air to fuel ratio is kept constant while changing fuel properties or not. Both the cases were simulated with blended fuel i.e. one with constant normalized air/fuel ratio and other by just keeping total flow rate constant.

Shown in Figure 10 is the simulated results obtained with different ethanol-gasoline blends. The total volumetric flow rate (air + fuel) was kept constant, and at the same time, the normalized air/fuel ratio is also maintained constant ($\lambda = 1$) as the fuel composition is changed by increasing the blending percentage from 0 to 100. The $(\text{Air/Fuel})_{\text{stoichiometry}}$ for ethanol is 8.95, whereas that for gasoline is 14.6. The fuel mixture used to simulate gasoline in this work has the corresponding ratio value of 15.03. Thus, if pure gasoline is blended with ethanol, the amount of air required for stoichiometric burning reduces. So as to compensate, the fuel flow rate need to be increased and air flow reduced to obtain the same total flow rate. Therefore, from Figure 10b, it is observed that the peak temperature is almost constant (0.1% variation), even though fuel composition is changed from 0 to 100% ethanol. This is because of the presence of more moles of fuel, which compensates for low heat of reaction as the blending % increases. The model predicts the qualitative trends correctly. The NO_x, HC, and CO emissions decrease continuously with increase in blending. From the plot of normalized reaction rate vs temperature (Figure 11a), it can be observed that the ethanol reaction rate being higher than other hydrocarbon is consumed first, even before peak temperature is reached. Thus, CO is formed earlier in the ethanol blended fuel that consumes oxygen present to get oxidized. Hence, compared to pure gasoline combustion, nitrogen has relatively less oxygen available when the required temperature for NO formation is reached. Figure 11 confirms that CO oxidation rate has increased and N_2 oxidation rate reduced, leading to decrease in NO_x formation and decrease in unburned hydrocarbon and CO emission.

Shown in Figure 12 is the effect of blending on emissions for the case where air to fuel ratio was kept constant at 15.03 (corresponds to $\lambda = 1$ for the 0% ethanol blending of gaseous mixture used here to represent gasoline) while increasing the ethanol blending from 0 to 100%. The simulated results agrees qualitatively with the experimental work presented in literature[16] where it is shown that HC and CO decrease while NO_x increases for the range 0 to 12% blending with ethanol. This model shows NO_x increases upto about 10% ethanol blending, after which the NO_x starts to decrease. As the stoichiometric air/fuel ratio required for ethanol is much lower than gasoline, the system becomes leaner if we increase the blending ratio without changing the air and fuel flow rate. Thus, we observe the same kind of trend as exhibited by leaner air–fuel mixtures. The CO and total HC emission decreases with increase in blending percentage, while NO_x shows a maxima as obtained with change in air-fuel ratio. At very high blending, there is slight increase in HC concentration which may be due to misfire. The peak temperature and pressure decreases with blending because of lower heat of combustion of ethanol when compared to gasoline.

Effect of engine load and speed

Shown in Figure 13 is the simulation result of the effect of change in load on engine emission, temperature and pressure at constant rpm and other engine parameters. The hydrocarbon reduces slightly while the NO_x emission increases with increase in load. The results obtained match with the trends reported in literature.[1] As the engine load increases, the amount of air and fuel entering the cylinder increases (for constant λ). This leads to increase in in-cylinder temperature and pressure leading to increase in NO_x and drop in hydrocarbon emission. Simulations were also performed keeping the load constant and varying rpm (Figure 14). The NO_x emission was observed to decrease while the HC emission increased. While this is in contrast to what is generally observed, it may be because we are keeping other parameters constant irrespective of the change in rpm. As the rpm increases, it can be noted from Eq. 9 that the volumetric flow rate into the cylinder increases and at the same time increase in rpm implies reduced residence time. Thus, we see a drop in temperature as rpm increases, and this leads to decrease in NO_x emission. For higher rpm, however, the model predicts increase in temperature and decrease in HC emission with rpm, which occurs because at higher rpm the time available for heat transfer per cycle by the coolant reduces leading to increase in in-cylinder temperature which compensates for increase in air-fuel flow rate.

Sensitivity of model

Sensitivity ($\frac{\partial X_i}{\partial p_j}$) is defined as how a desired output (X_i : peak temperature, peak pressure, exit concentration of

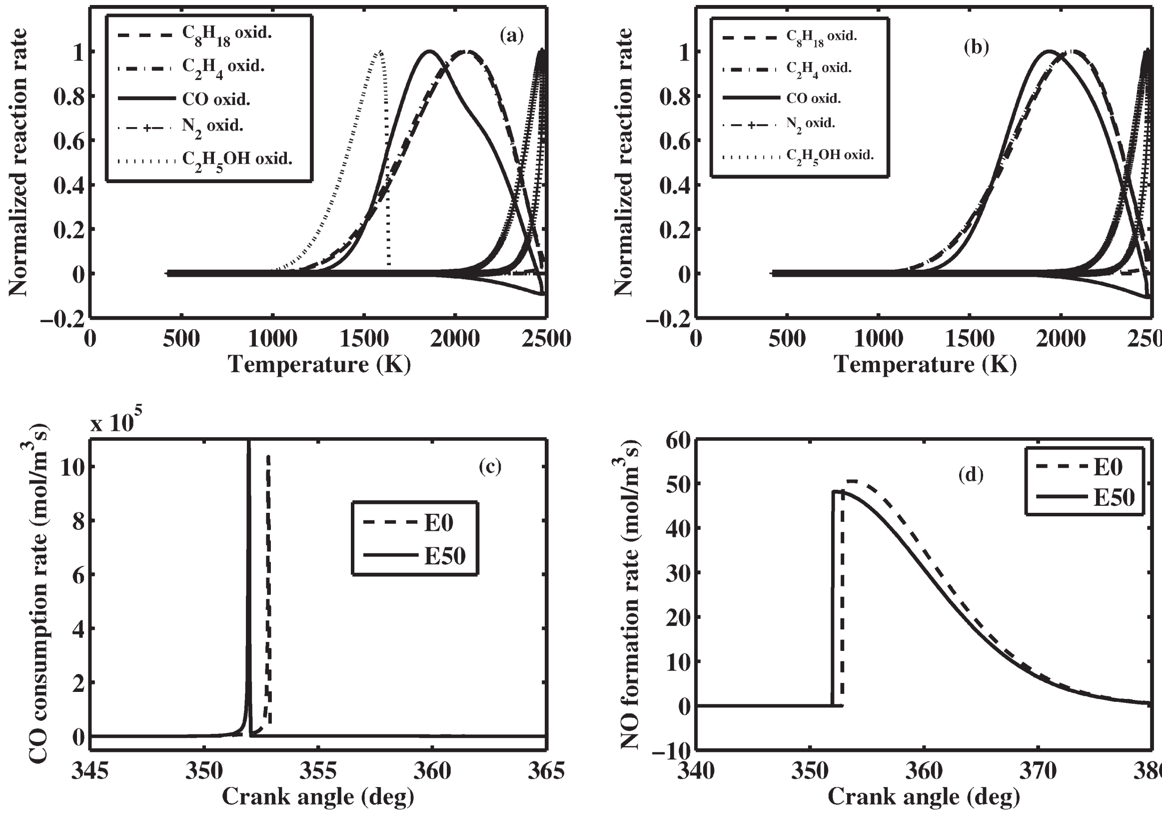

Figure 11. Comparison of reaction rate during a cycle for E0 and E50 (a) normalized reaction rate for 50% ethanol (vol%) blended gasoline, (b) normalized reaction rate for gasoline, (c) CO oxidation rate, and (d) NO_x formation rate.

hydrocarbon, CO and NO_x) varies with system parameters (p_j) like dimensionless mixing time ($\tau_{\mathrm{mix},1}$), crevice volume, spark timing and duration, compression ratio, feed composition, kinetic parameters etc. In this section, we examine briefly the sensitivity of the cycle simulation results to the values of selected parameters.

Sensitivity to Mixing Time. In the base case model considered in this work, there is no valve overlap. Thus, $\tau_{\mathrm{mix},2} = 0$ for all the stages in engine cycle and $\tau_{mix,1} \neq 0$ only during the exhaust stroke and was chosen as 0.2. $\tau_{\mathrm{mix},1}$ being positive, it can be seen from Eq. 49, shown in Appendix A, that cup mixing concentration is lower than volume averaged concentration. Increasing the mixing time $\tau_{\mathrm{mix},1}$ implies that the concentration inside the cylinder is higher when compared to the fluid leaving the system. This also agrees with what is expected intuitively as it will take finite time for the reactant to mix uniformly. So near the exhaust port as the gases exit the reactor, concentration should drop and will become lower than the averaged concentration in the reactor. The effect of increasing $\tau_{mix,1}$ is similar to that of increasing the internal exhaust gas recirculation (EGR), as higher mixing time implies more gases are left behind in the cylinder. The combustible leftover gases act like a diluent (or inert), increasing the specific heat of the system thereby reducing the temperature inside the cylinder. As NO formation is very sensitive to temperature change, the concentration of NO_x drops as the mixing time increases. The HC conversion is a weak function of $\tau_{\mathrm{mix},1}$ and reduces a little while CO is almost unchanged. The peak temperature drops as mixing time increases because of increase in EGR fraction, whereas the peak pressure remains almost unchanged as a result of two competing effects of decrease in the temperature and increase in reactant moles. Shown in Figure 15 is the influence of mixing time $\tau_{\mathrm{mix},1}$ on emissions, as well as, peak temperature and pressure.

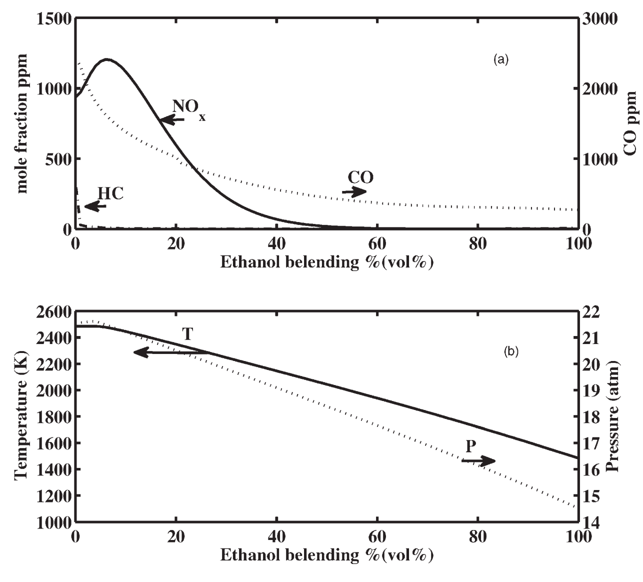

Figure 12. Impact of blending on (a) emissions and (b) in-cylinder temperature and pressure under constant air-fuel ratio condition (λ goes leaner).

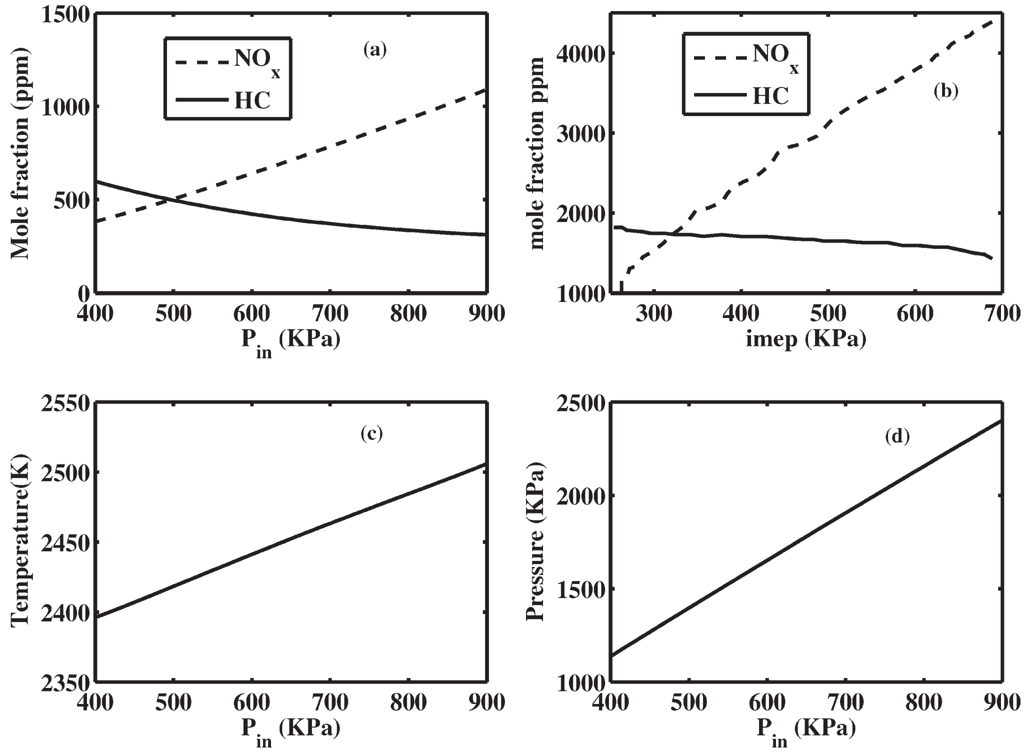

Figure 13. (a) Impact of change in load on engine emissions as predicted by model, (b) experimentally observed variation in emissions,[1] (c) in-cylinder peak temperature variation with load, and (d) effect of load on in-cylinder peak pressure.

It may be noted that in the limit $\tau_{mix,1} \rightarrow 0$, the model reduces to a classical one-mode ideal combustion chamber model with $C_m = \langle C \rangle$. As stated earlier, though this one-mode model can also be used to predict the basic trends qualitatively, it predicts peak temperature and NO_x emission that are higher than observed (Figure 16). Hase et al.[20,21] reported that the NOx emission increase with increase in mixedness around stoichiometric, and the two mode model explains that behavior. Also, as the one-mode model assumes complete mixing or uniform concentration within the reactor, it does not capture the effect of valve location or is not suitable for cases where large gradients exists like in the direct injection system, and thus, a two mode model is required for better prediction. The extension of the model to include the valve overlap case, where $\tau_{mix,2} \neq 0$ will be examined in future work.

Sensitivity to Crevice Volume. The crevice is one of the main reasons for unburned hydrocarbon, other reason being wall quenching and incomplete combustion.[1] Because of its high surface to volume ratio, the temperature in the crevice is close to wall temperature, which is much cooler as compared to gases in the reactor. During the compression stroke and combustion period, when the reactor pressure is high, some of the gases escapes into the crevice avoiding primary combustion. Increasing the crevice volume increases its capacity to store unburned gases thus leading to increase in unburned hydrocarbon emission. By trapping some of unburned hydrocarbon, it also reduces the peak temperature and leads to a small drop in NO_x and CO emissions. Shown in Figure 17 is the sensitivity of model prediction as the crevice volume is increased from 0 to 5% of the clearance volume. Similarly, reducing the crevice flow rate coefficient ($Q_{cr,0}$) reduces the unburned hydrocarbon at exit.

Sensitivity to Spark Duration and Timing. In our model, the spark is activated between 12 to 8.5 degree BTDC with a rate of 1.4×10^5 J/s which approximates to an energy input of 54.76 J for engine rotating at 1500 rpm. The above value for the heat rate would be much lower if a compartment type model is considered because in that case the spark is required to ignite just the nearby gases and then the flame front will propagate. However, in the present model, higher energy input by spark is required as all mass ignites at once. Still the amount of heat added by the spark is a small fraction when compared to the amount of heat produced by combustion. Keeping the total amount of energy added by the spark constant and reducing the duration and energy rate accordingly leads to earlier start of ignition when compared to slow spark, and the unburned hydrocarbon decreases and NO_x emission increases. A 3.5 times shorter ignition duration resulted in around 10% reduction in hydrocarbon emission and around 5% increase in NO_x. Spark timing also influences the peak temperature and pressure. For example, by advancing the spark timing so that spark is ignited 1^0 earlier resulted in a slight increase in temperature and led to around 2.5% increase in NO_x and simultaneous decrease of around 3–4% in hydrocarbon emission. The CO emission was almost insensitive. Similarly, for spark retard, i.e., ignition time moved closer to top dead center (TDC) led to decrease in NO_x and increase in hydrocarbon emission. The trend observed matches the one reported in literature.[1]

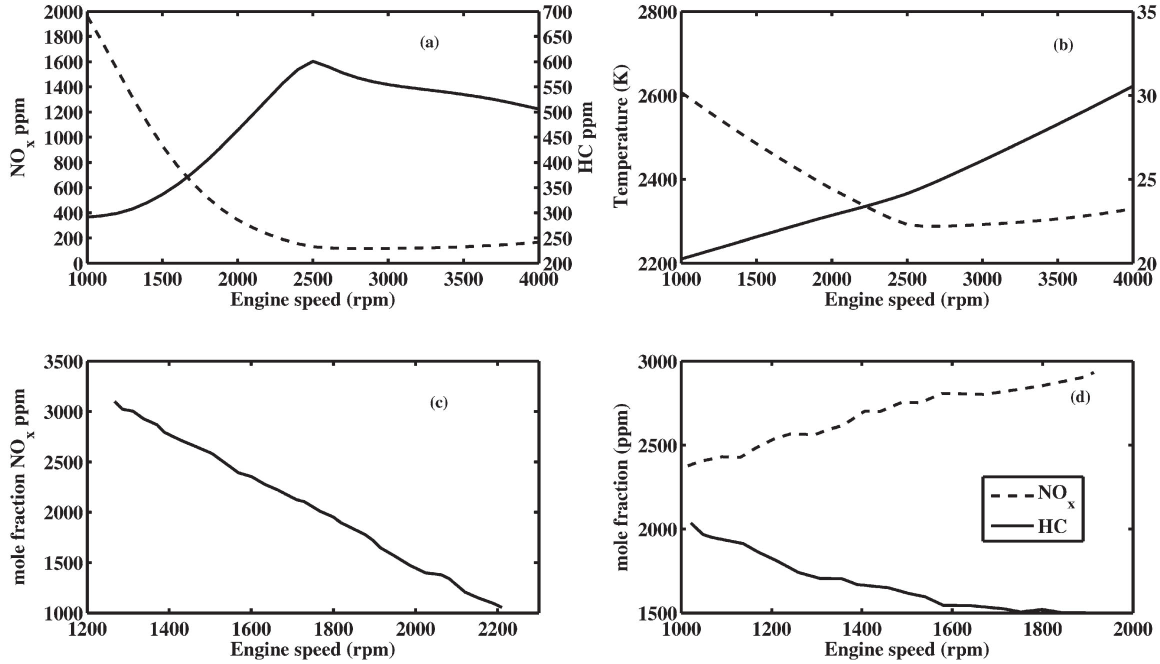

Figure 14. Impact of engine speed on (a) NO_x and HC emission as predicted by model, (b) in-cylinder peak temperature (dashed curve) and peak pressure, (c) experimentally reported NO_x with change in speed at A/F=16.9 for gasoline fuel,[19] and (d) experimentally reported HC and NO_x with change in engine speed.[1]

Sensitivity to Reaction Kinetics. As can be expected, emissions are strong function of the combustion kinetics used. When the gasoline is represented as single lump although the NO_x emission, temperature and pressure trend could be predicted quite accurately using the low dimensional model developed here, the hydrocarbon emission was under determined. Thus, a two lump gasoline model was selected with 80% fast burning and 20% slow burning. As stated in the introduction, the prediction of hydrocarbon emission could be improved by using a five or six lump model of gasoline and a more detailed kinetic model for combustion of each class of hydrocarbon. However, as the goal of study was to use a simple non trivial model, we lump hydrocarbon as fast burning and slow burning and use the kinetics available in literature for prediction. Iso-octane being the typical representation for gasoline was used as the major component. As for slow burning, the combustion kinetics slower than octane combustion was used. A 10% increase in the rate of slow burning component results in a decrease of unburned hydrocarbon emission by $\sim$10% while it has very little effect on NO_x emission, decreasing its value by just around 1%. Small change ($\pm$ 5%) in rate of reaction for fast burning component does not influence emissions much.

Sensitivity to Feed Inlet Temperature. Shown in Figure 18 is the effect of inlet temperature on emission and in-cylinder temperature and pressure. The in-cylinder temperature increases, as expected, but the sensitivity is low this is because the feed gas (air + fuel) enters the cylinder at a temperature in the order of 300 K while the gases left within the cylinder from earlier combustion cycle are at much higher temperature around 1000 K. Also, since the inlet temperature is higher, keeping the heat supplied by spark constant, leads to early ignition (ignition delay time reduces). The hydrocarbon emission increases by around 3% for 10% increase in feed temperature (compared to ambient conditions) and the NO_x emission shows around 4% increase. The peak in-cylinder pressure decreases with increase in temperature because at constant inlet pressure condition, increase in inlet temperature leads to decrease in inlet concentration.

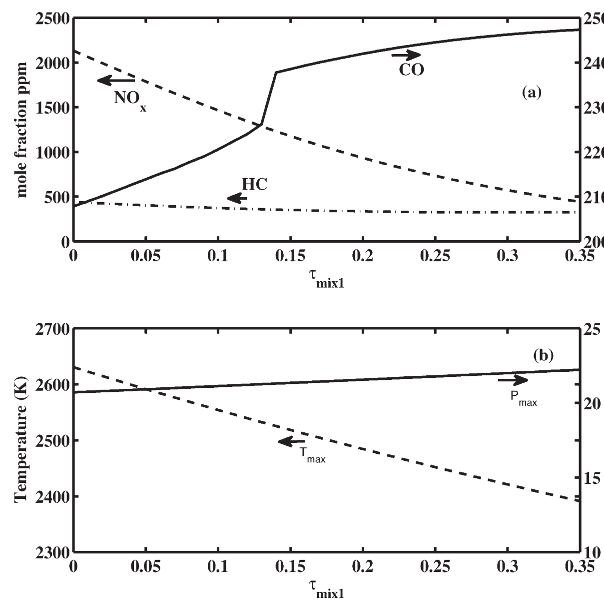

Figure 15. Influence of in-cylinder dimensionless mixing time on (a) emissions and (b) in-cylinder peak temperature and peak pressure.

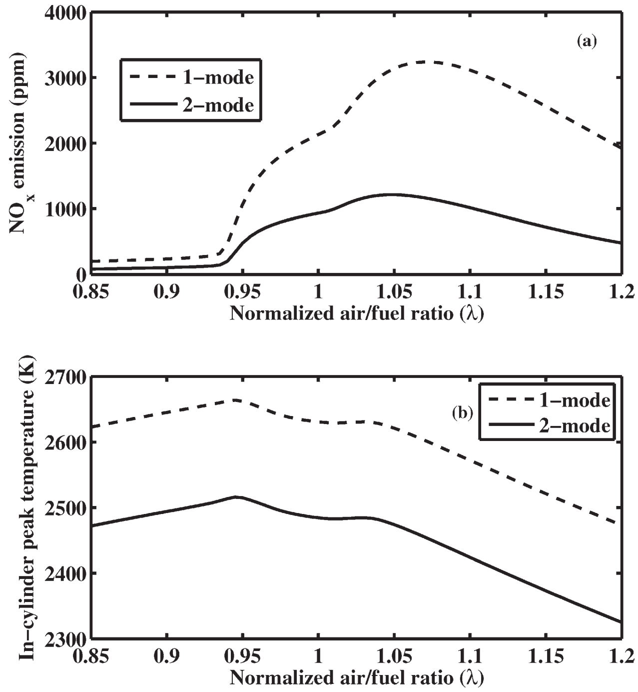

Figure 16. Comparison between one mode (completely mixed) and two mode (unmixed) ($\tau_{mix,1}$ = 0.2 and $\tau_{mix,2}$ = 0) model (a) NOx emission with change in normalized air to fuel ratio (b) in-cylinder peak temperature with change in normalized air to fuel ratio.

Extensions to the Low-Dimensional Combustion Model

The main goal of this work was to provide a first principles - based low-dimensional in-cylinder combustion model so that it may be coupled with a exhaust after-treatment model and control schemes for real-time simulation and optimization of the overall system. Thus, we have presented only the simplest non trivial model that retains the main qualitative features of the in-cylinder combustion process. The model presented here can be extended to homogeneous charge compression ignition (HCCI), gasoline direct injection (GDI), or variable valve timing (VVT) engines. In addition, the model predictions can be improved (at the expense of increased complexity and computational time) by relaxing the various assumptions. A few of these extensions are discussed below in more detail.

Extensions to the combustion chamber model

In the preliminary model studied here, after averaging the model is reduced to a single compartment. Thus, we do not see the ignition delay, which will appear if we extend the single compartment model to multi compartment model or use multiple-temperature and concentration modes to account for the spatial variations. This extension will also improve the model prediction for ignition delay.

In this work, hydrocarbon oxidation kinetics considered here, takes conversion of hydrocarbon directly to CO. But to capture the hydrocarbon and CO emission more properly, we need to extend the kinetics to include reactions involving conversion of heavier hydrocarbons to intermediate lighter smaller hydrocarbons. This will increase the number of ODEs to be integrated and requires the kinetics of oxidation

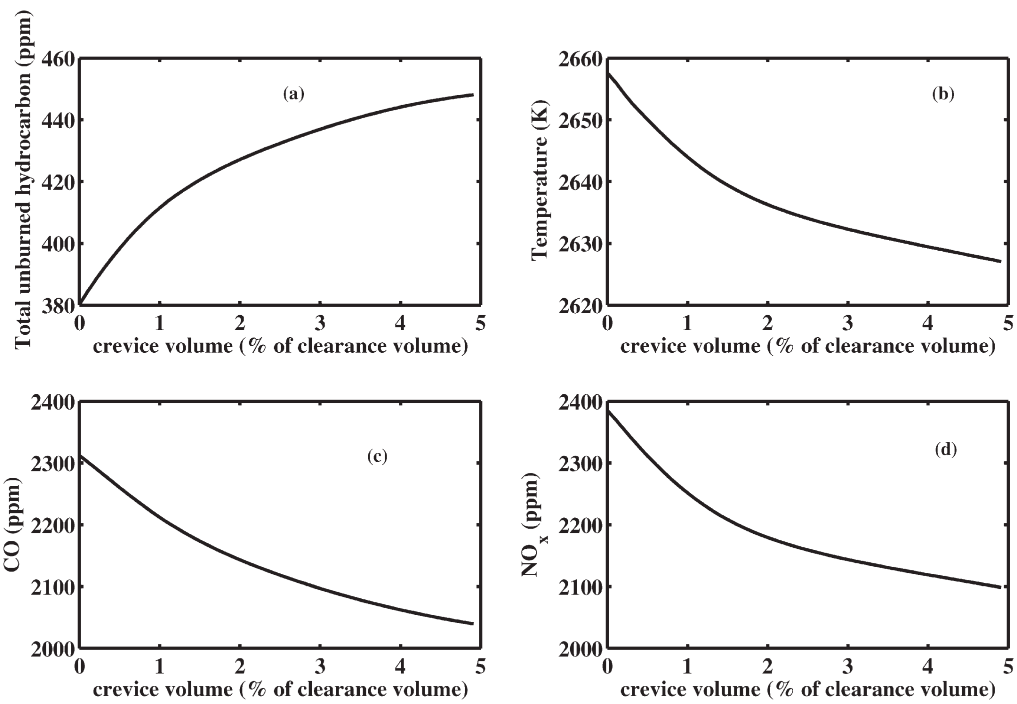

Figure 17. Impact of change in crevice volume on (a) hydrocarbon emission, (b) in-cylinder peak temperature, (c) CO emission, and (d) NO$_x$ emission for $\tau_{mix,1}$ = 0 and $\tau_{mix,2}$ = 0.

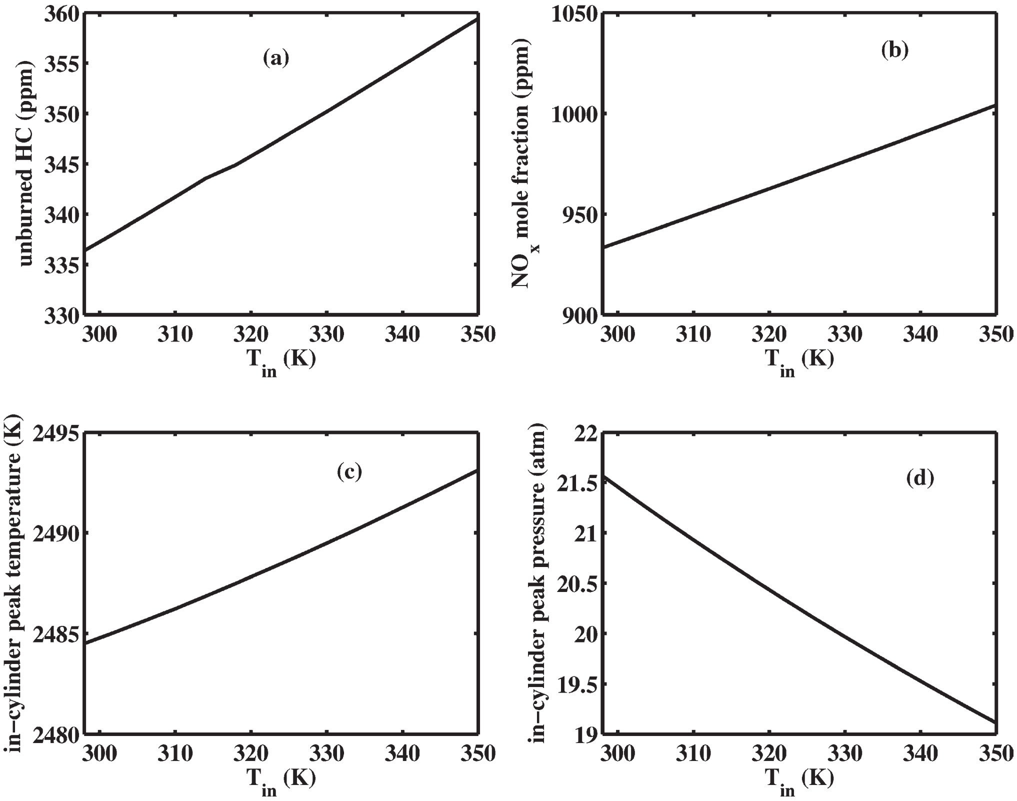

Figure 18. Impact of change in inlet temperature on (a) hydrocarbon emission, (b) NO_x emission, (c) in-cylinder peak temperature, and (d) in-cylinder peak pressure.

of the different lumps but can improve the CO and HC emission predictions.

Also, in thus model, the valve overlap was not considered. The presence of valve overlap is expected to reduce NO_x emission and increase hydrocarbon prediction. This is because, valve overlap leads to some flow of combustion gases to intake manifold, leading to an effect similar to internal EGR and thus should lead to decrease in system temperature. To include this extension, two more control volumes (exhaust and inlet manifold) will need to be clubbed with the present combustion model.

Torque model

In this work, the engine speed is assumed constant. However, in a real system, the engine speed is a function of mass air flow or the engine load. To quantify this, we can use the torque balance given by[22]

$$I\frac{d\Omega(t)}{dt} = T_{\rm e}(t) - T_{\rm l}(t), \tag{23}$$

where $T_{\rm e}$ and $T_{\rm l}$ represents the effective torque (toque measured on the engine shaft) and load torque, respectively. The engine torque has been modeled in literature[22] as

$$T_{\rm e}(t) = \eta_{\rm e}\frac{\dot{m}_f Q_v}{2\pi\Omega}, \tag{24}$$

where $Q_{\rm v}$ is the heating value of gasoline, and $\eta_{\rm e}$ is an experimentally determined value to represent combustion and torque effective efficiency. The load torque can be determined from transmission and driveline model,

$$F_{\rm v}v_{\rm v} = 2\pi\Omega T_l\eta_{\rm m}, \tag{25}$$

where $F_{\rm v}$ is the force acting on the wheel of the vehicle and $v_{\rm v}$ is the vehicle velocity and $\eta_{\rm m}$ is the power transmission efficiency,

$$v_{\rm v} = R_{\rm w}\frac{2\pi\Omega}{i_D i_G}, \tag{26}$$

where $R_{\rm w}$ is the radius of the wheels, $i_{\rm D}$ and $i_{\rm G}$ are the reduction ratio of the differential and the reduction ratio of the gearbox, respectively. The vehicle model is

$$F_{\rm v} = M_{\rm v}\frac{dv_{\rm v}}{dt} + SC_x\frac{\rho_a v_v^2}{2} + f_r M_{\rm v} g\cos\phi + M_{\rm v} g\sin\phi, \tag{27}$$

where $M_{\rm v}$ is the mass of the vehicle, S is the frontal surface of the vehicle, C_x is the drag coefficient of the vehicle, ρ_a is the density of air, f_r is the friction coefficient, and ϕ is the slope of the road. By combining the above torque model with the combustion model, the emissions produced over a specific drive cycle can be simulated. This will be pursued in future work.

Controller design

Most gasoline engines are controlled by throttling the air into the intake manifold. The control over which the driver has direct control is the throttle angle plate. We can implement our first principle-based low-dimensional model in the current controller scheme. The system input will be throttle angle and speed based on which the model will compute the required fuel flow rate and exhaust gas composition after combustion. This will give us λ which can be used for closed loop controller design.

Summary and Discussion

As stated in the introduction, the main goal of this article was to develop a fundamentals-based low-dimensional in-cylinder combustion model that can predict the composition of the regulated exhaust gases as a function of the various design and operating variables. The low-dimensional model developed involves total of 10 different species and consist of mole (or mass) balance for each species in crevice and cylinder and an energy balance for a total of 21 ODEs. The model is then verified for different operating conditions and was observed to agree qualitatively with the results reported in the literature. The basic findings and assumptions can be summarized as follows: (i) out of all the regulated emissions, NO_x formation is most sensitive to peak temperature and occurs at very high temperature (above 1800 K), (ii) CO and hydrocarbon emission decreases with increase in air-fuel ratio (λ) whereas the NO_x exhibits a maxima occurring at slightly leaner mixture conditions, (iii) ethanol blending decreases CO and hydrocarbon emissions, while NO_x emission may be higher or lower depending on the mode of operation, (iv) reducing the crevice volume can reduce the unburned hydrocarbon emissions, (v) advancing the spark timing will lead to increase in NOx emissions. Model assumptions: (a) All the fuel injected is assumed to enter the cylinder and undergoes combustion: This is simplification of the real system in which not all the fuel evaporates and some stick to the intake valves, while some leftover from earlier cycle may evaporate adding purge, (b) fuel and air mixture are treated as an ideal gas, (c) fuel and air gets premixed before entering the cylinder, (d) engine speed is assumed constant, (e) there is no valve-overlap, and hence backflow of gases from cylinder to the intake manifold.

We have demonstrated that the model presented here, though preliminary, is the simplest non trivial model that has the correct qualitative features. As discussed above, the quantitative predictions of the model can be improved by extending the model and relaxing some of the assumptions. Based on the sensitivity results presented, the quantitative features of the model can also be fine tuned to any specific IC engine design or specific mode of operation. For simplicity, this work considered only the case of port injection with pre mixed feed. However, the present approach may be extended to include mixing limitations outside of the cylinder (before the air-fuel mixture enters the in-take valve). The model can also be extended to direct injection and other such operating conditions.

One main reason for the development of the low-dimensional in-cylinder combustion model is our desire to integrate it with the engine load/torque model and couple it to the exhaust after-treatment models and control schemes. In our recent work, we have also developed low-dimensional models for real time simulations of various after-treatment systems such as three-way catalytic converters (TWCs) and lean NOx traps (LNTs).[23] As stated in the introduction, while each of the sub system models have been studied in the literature, to our knowledge, the behavior of the integrated system and system level optimization has not been studied. This system level integration and optimization will be pursued in the future work.

Acknowledgments

This work is supported by NSF grant (CMMI 0727999) and the Ford Motor Company.

Notation

a = crevice flow parameter
A_{th} = throttle area, m^2
B = cylinder bore, m
$\langle C \rangle$ = volume averaged concentration, mol/m^3
C_{cr} = concentration within crevice region, mol/m^3
C_d = drag coefficient
C_m = flow averaged concentration, mol/m^3
C_x = vehicle drag coefficient
E = experimentally determined constant
f_r = friction coefficient
F = exit molar flow rate, mol/s
F^{in} = inlet molar flow rate, mol/s
F_{cr} = crevice exchange flow rate, mol/s
F_v = force on the vehicle wheel, N
g = acceleration due to gravity, m/s^2
$h_{c,c}$ = coolant side heat transfer coefficient, W/(m^2 K)
$h_{c,g}$ = gas side heat transfer coefficient, W/(m^2 K)
H_j^{in} = molar enthalpy of component j at inlet conditions, J/mol
H_j = molar enthalpy of component j at exit conditions, J/mol
$\Delta H_{R,T}$ = heat of reaction computed at temperature T, J/mol
i = reaction index
I = moment of inertia of the powertrain, Kg m^2
i_D = reduction ratio of the differential
i_G = reduction ratio of the gearbox
j = component number
k = thermal conductivity of wall, W/(m K)
l = cylinder wall thickness, m
l_c = clearance length, m
$\dot{m}_f$ = fuel mass flow, kg/s
M_v = mass of the vehicle, kg
N_c = total number of components/ species
N_R = total number of reactions
P = in-cylinder pressure, Pa
$P_{crevice}$ = crevice pressure, Pa
P_{out} = downstream pressure, Pa
Q = exit volumetric fuel flow rate, m^3/s
Q_{in}^{fuel} = inlet volumetric fuel flow rate, m^3/s
Q_{in}^{air} = inlet volumetric air flow rate, m^3/s
Q = energy added by spark, J/s
Q_{cr} = crevice volumetric flow rate, m^3/s
Q_v = heating value of fuel, J/Kg
R = universal gas constant, 8.314 J/(K mol) or ($m^3 Pa$)/(K mol))
$\hat{R}$ = ratio of connecting rod length to crank radius
$R(\langle C \rangle)$,$R(C_{cr})$ = reaction rate at concentration $\langle C \rangle$, C_{cr}, mol/(m^3s)
r_c = compression ratio
R_w = radius of the wheels, m
S = frontal vehicle surface, m^2
S_p = mean piston speed, m/s
t = instantaneous time, s
T = average bulk gas temperature, K
T_c = coolant temperature, K
$T_{w,c}$ = coolant side wall temperature, K
$T_{w,g}$ = gas side wall temperature, K
T_e = effective toque, N m
T_l = load torque, N m
$t_{mix,i}$ = ith mixing time
V = instantaneous volume of cylinder, m^3

V_c = clearance volume, m^3
V_{cr} = crevice volume, m^3
V_d = displaced or swept volume, m^3
V_R = total volume of the cylinder, m^3
v_v = vehicle velocity, m/s
w = average cylinder gas velocity, m/s
x_e = ethanol mole fraction
λ = ratio Air/ fuel actual to that at stoichiometry
θ = crank angle, rad
ϕ = slope of road, rad
Ω = angular speed, rad/s
v_{ij} = stoichiometric coefficient of ith reaction and jth component
ρ = density of in-cylinder gaseous mixture, kg/m^3
ρ_a = density of air, kg/m^3
γ = heat capacity ratio
σ = Stefan -Boltzman constant, $W/(m^2K^4)$
ε = emissivity
η_e = effective efficiency
η_e = volumetric efficiency
η_m = power transmission efficiency

Literature Cited

1. Heywood JB. *Internal Combustion Engine Fundamentals*. New York: McGraw-Hill, Inc., 1988
2. Blumberg PN, George AL, Rodney JT. Phenomenological models for reciprocating internal combustion engines. *Prog Energy Combust Sci*. 1979;5:123–167.
3. Verhelst S, Sheppard CGW. Multi-Zone thermodynamic modelling of spark-ignition engine combustion-overview. *Energy Convers Manage*. 2009;50:1326–1335.
4. Bayraktar H, Durgun O. Mathematical modelling of spark-ignition engine cycles. *Energy Sources*. 2003;25:651–666.
5. Bhattacharya M, Harold MP, Balakotaiah V. Low-dimensional models for homogeneous stirred tank reactors. *Chem Eng Sci*. 2004;59: 5587–5596.
6. Curran HJ, Gaffuri P, Pitz WJ, Westbrook CK. Comprehensive modeling study of iso-octane oxidation. *Combust Flame*. 2002;129:253–280.
7. Westbrook CK, Dryer FL. Simplified reaction mechanisms for the oxidation of hydrocarbon fuels in flames. *Combust Sci Technol*. 1981;27:31–43.
8. Jones WP, Lindstedt RP. Global reaction scheme for hydrocarbon combustion. *Combust Flame*. 1988;73:233–249.
9. Marinov NM, Westbrook CK, Pitz WJ. Detailed and global chemical kinetics model for hydrogen. In 8th International Symposium on Transport Properties, San Francisco, CA, 1995.
10. Franchek MA, Mohrfeld J, Osburn A. Transient fueling controller identification for spark ignition engines. *J Dyn syst Meas Control-Trans ASME*. 2006;128:499–509.
11. Carpenter MH, Ramos JI. Mathematical modelling of spark-ignition engines. *Appl Math Modell*. 1985;9:40–52.
12. Smith JM, Van Ness HC, Abott MM. *Introduction to Chemical Engineering Thermodynamics*, 6th ed. New York: Tata McGraw-Hill, 2003.
13. Heck RM, Farrauto RJ, Gulati ST. *Catalytic Air Pollution Control: Commercial Technology*. New York: John Wiley, 2002.
14. Kumar P. Fundamentals-Based Low-Dimensional Combustion and After-Treatment Models for Gasoline Engines. Doctoral dissertation, University of Houston, Houston, TX, 2011.
15. Najafi G, Ghobadian B, Tavakoli T, Buttsworth DR, Yusaf TF, Faizollahnejad M. Performance and exhaust emissions of a gasoline engine with ethanol blended gasoline fuels using artificial neural network. *Appl Energy*. 2009;86:630–639.
16. Bayraktar H. Experimental and theoretical investigation of using gasoline–ethanol blends in spark-ignition engines. *Renewable Energy*. 2005;30:1733–1747.
17. Celik MB. Experimental determination of suitable ethanol–gasoline blend rate at high compression ratio for gasoline engine. *Appl Thermal Eng*. 2008;28:396–404.
18. Koc M, Sekmen Y, Topgul T, Yucesu HS. The effects of ethanol–unleaded gasoline blends on engine performance and exhaust emissions in a spark-ignition engine. *Renewable Energy*. 2009;34:2101–2106
19. Sodré JR. Modelling NO_x emissions from spark-ignition engines. *Proc Inst Mech Eng D- J Automobile Eng*. 2000;214:929–934.
20. Hase K, Kori Y, Ohgl K. Effect of Air/Fuel ratio fluctuation on the formation of nitrogen oxides. *Combust Technol Clean Environ*. 1995;1:815–824.
21. Hase K, Kori Y. Effect of premixing of fuel gas and air on NO_x formation. *Fuel*. 1996;75:1509–1514
22. Saerens B, Vandersteen J, Persoons T, Swevers J, Diehl M, Bulck EV. Minimization of the fuel consumption of a gasoline engine using dynamic optimization. *Appl Energy*. 2009;86:1582–1588.
23. Joshi SY, Harold MP, Balakotaiah V. Low-dimensional models for real time simulations of catalytic monoliths. *AIChE J*. 2009;55: 1771–1783.

Appendix A: Derivation of the Low-Dimensional In-Cylinder Combustion Model

In recent work, Bhattacharya et al.[5] have developed a low-dimensional model for homogeneous stirred-tank reactors by averaging of the full three dimensional convection-diffusion-reaction (CDR) equation for the isothermal case. In the first step of their approach, the reacting volume is divided into N cells (where N can be arbitrarily large), and the Liapunov-Schmidt technique is used to coarse-grain the CDR equation at the meso scale over each cell. In the second step, this interacting cell model is further reduced to a two-mode model consisting of a single differential equation and an algebraic equation relating the two concentration modes (the cup-mixing concentration, C_m, and the volume averaged concentration, $\langle C\rangle$). For example, for case in which the inlet and exit flow rates and reactor volume are independent of time, the two-mode model may be written as

$$\frac{d\langle C\rangle}{dt'} + R(\langle C\rangle) = \frac{1}{\tau}\left(C_m^{\text{in}} - C_m\right),$$

$$C_m - \langle C\rangle = \frac{1}{\tau}\left(t'_{\text{mix},2}C_m^{\text{in}} - t'_{\text{mix},1}C_m\right),$$

where τ is the residence time, $t'_{\text{mix},1}$ is the overall mixing time in the tank, which depends on the local variables (such as local velocity gradients, local diffusion length, diffusivity) as well as reactor scale variables while $t'_{\text{mix},2}$ captures the effect of nonuniform feeding of the reactants. When both mixing times are zero, $C_m = \langle C\rangle$ and the above model reduces to the classical ideal one-mode CSTR model. It was shown by Bhattacharya et al. that when $0 < \frac{t_{\text{mix},2}}{\tau} \ll 1$, the above two-mode model has the same qualitative features as the full CDR equation. In general, the mixing times $t'_{\text{mix},1}$ and $t'_{\text{mix},2}$ depend on molecular properties as well as the flow field and reactor geometry and other factors (such as the locations of inlet and exit streams, baffle positions, and stirrer speed.) and may be expressed as

$$t'_{\text{mix},1} = \underbrace{\tau_m\alpha_1}_{\text{micromixing}} + \underbrace{\tau_M\alpha_2}_{\text{macromixing}}, \tag{A1}$$

$$t'_{\text{mix},2} = \underbrace{\tau_m\alpha_3}_{\text{micromixing}} + \underbrace{\tau_M\alpha_4}_{\text{macromixing}}, \tag{A2}$$

where τ_m is the characteristic local scale mixing (also called micromixing) time present within the tank (which depends on the molecular properties such as species diffusivities), whereas τ_M is the characteristic large scale (or macromixing) time in the tank (which depends on the flow field and other macro variable mentioned above]. The numerical coefficients α_i, $i = 1,2,3,4$ depend on reactor geometry as well as feed and exit stream distributions. It should be noted that it is the overall mixing times that enter the final averaged model and not the individual (micro and macro) contributions. However, based on the typical characteristic values of τ_m and τ_M, both micro and macro mixing contributions may be important for liquid phase reactions, whereas macromixing may be dominant for gas phase reactions.

We extend the above approach for the case of IC engines with the following assumptions: (i) N interacting cells, (ii) exchange or circulation flow between cells is much larger than inlet or exit flow at any time, (iii) even though the total volume varies with time, the relative volume fractions of the cells remain constant. Based on operational conditions IC engine cycle is divided into 3 stages

1. only intake valve open
2. both valves closed
3. exhaust valve open

Case 1 and 3 represent semi batch condition, with only intake and exhaust flow, respectively. Case 2 corresponds to batch operation condition. Model development is first discussed for a general case and then special cases are discussed.

[Note: Bold letters represent vectors/matrices while scalars are written in normal font.]

In a matrix form, we can write mass balance for N number of interacting perfectly mixed cells as,

$$\frac{d}{dt}(\mathbf{V}_R(t)\mathbf{C}(t)) = \mathbf{Q}_{in}(t)\mathbf{C}_{in}(t) - \mathbf{Q}_e(t)\mathbf{C}(t) + \mathbf{Q}(t)\mathbf{C}(t) - \mathbf{V}_R(t)\mathbf{R}(\mathbf{C}), \quad \text{(A3)}$$

where,

$$\mathbf{V}_R = \begin{Bmatrix} V_i & ,i=j \\ 0 & ,i\neq j \end{Bmatrix} \quad \mathbf{Q} = \begin{Bmatrix} -\Sigma_{j=1,i}^{n} Q_{ij}^c & ,i=j \\ Q_{ji}^c & ,i\neq j \end{Bmatrix}$$

$$\mathbf{Q}_{in} = \begin{Bmatrix} Q_i^{in} & ,i=j \\ 0 & ,i\neq j \end{Bmatrix} \quad \text{and} \quad \mathbf{Q}_e = \begin{Bmatrix} Q_i^{ex} & ,i=j \\ 0 & ,i\neq j \end{Bmatrix}$$

where, $\mathbf{V}_R \in \mathbb{R}^{N\times N}$ and V_i is the volume of ith cell, $\mathbf{C} = [C_1\ C_2.....]^T \in \mathbb{R}^{N\times 1}$ where C_i is the spatially averaged concentration of each cell. $\mathbf{Q}$, $\mathbf{Q}_{in}$ and $\mathbf{Q}_e \in \mathbb{R}^{N\times N}$, Q_{ij}^c is the circulation flow rate from cell i to cell j, Q_i^{in} and Q_i^{ex} are the inlet and exit flow from ith cell, respectively. The reaction rate vector $\mathbf{R}(\mathbf{C}) \in \mathbb{R}^{N\times 1}$. The total volume of the reactor is given by, $V_R = \sum V_i$, and the fractional volume are defined as $\alpha_i = V_i/V_R$. Assume that although total volume is a function of time, each cell volume changes proportionately such that relative volume fraction remains constant. Thus $\mathbf{V}_R(t) = V_R(t)\,\boldsymbol{\alpha}$. Rearranging Eq. A3 we get,

$$\mathbf{Q}(t)\mathbf{C}(t) = \frac{d}{dt}(V_R(t)\boldsymbol{\alpha}\mathbf{C}(t)) + V_R(t)\boldsymbol{\alpha}\mathbf{R}(\mathbf{C}(t)) + \mathbf{Q}_e(t)\mathbf{C}(t) - \mathbf{Q}_{in}(t)\mathbf{C}_{in}(t). \quad \text{(A4)}$$

It may be noted that $\mathbf{Q}$ is a symmetric matrix with zero row and column sum. Thus, at any time t

$$\mathbf{Q}(t)\mathbf{y_0} = \mathbf{0}, \quad \text{(A5)}$$

with $\mathbf{y_0} = [1\ 1\ 1\ 1\ .....]^T$. Similarly, the adjoint (or left) eigenvector is given by

$$\mathbf{v_0}^T\mathbf{Q}(t) = \mathbf{0}, \quad \text{(A6)}$$

with $\mathbf{v_0}^T = [1\ 1\ 1\ 1\ .....]$. Let $\varepsilon = 1/\|\mathbf{Q}(t)\|$, then in the limit $\varepsilon \to 0$ (i.e. very fast circulation flow rate), from Eqs. A4 and A5 we get $\mathbf{C} = \langle C\rangle\mathbf{y_0}$ i.e. when circulation flow rate is very high, all the cells are in perfect communication and the concentration is uniform, given by $\langle C\rangle$. For small but finite ε, there exist a deviation from equilibrium state, the concentration then is given by

$$\mathbf{C} = \langle C\rangle\mathbf{y_0} + \mathbf{C}', \quad \text{(A7)}$$

where,

$$\mathbf{C}' = \varepsilon\mathbf{w}_1 + \varepsilon^2\mathbf{w}_2 + ... \quad \text{(A8)}$$

Lets define inner product as

$$\langle \mathbf{x}, \mathbf{y}\rangle \equiv \mathbf{y}^T\boldsymbol{\alpha}\mathbf{x}. \quad \text{(A9)}$$

where $\mathbf{x} \in \mathbb{R}^{N\times 1}$ and $\mathbf{y} \in \mathbb{R}^{N\times 1}$ and $\boldsymbol{\alpha} \in \mathbb{R}^{N\times N}$ is the volume fractions. The volume averaged concentration is defined as

$$\langle C\rangle = \langle \mathbf{C}, \mathbf{v_0}\rangle \equiv \mathbf{v}_0^T\boldsymbol{\alpha}\mathbf{C} = \frac{\sum_{i=1}^n V_iC_i}{\sum_{i=1}^n V_i}. \quad \text{(A10)}$$

Taking inner product of Eq. A7 with $\mathbf{v_0}$ and using result from Eq. A10 gives the solution to $\langle \mathbf{C}', \mathbf{v_0}\rangle$ as

$$\langle \mathbf{C}', \mathbf{v_0}\rangle = 0. \quad \text{(A11)}$$

Multiplying Eq. A4 by $\mathbf{v_0}^T$ on LHS and using Eq. A6 we get

$$0 = \mathbf{v_0}^T\left(\frac{d}{dt}(V_R(t)\boldsymbol{\alpha}\mathbf{C}(t)) + V_R(t)\boldsymbol{\alpha}\mathbf{R}(\mathbf{C}(t)) + \mathbf{Q}_e(t)\mathbf{C}(t) - \mathbf{Q}_{in}(t)\mathbf{C}_{in}(t)\right). \quad \text{(A12)}$$

Now simplifying,

Term 1: $V_R(t)\mathbf{v_0}^T\boldsymbol{\alpha}\mathbf{C}(t) = V_R(t)\langle C\rangle\mathbf{y_0}$

Term 2: $\mathbf{v_0}^T\ \boldsymbol{\alpha}\ \mathbf{R}(\mathbf{C}) = \mathbf{v_0}^T\alpha(\mathbf{R}(\langle C\rangle\mathbf{y_0}) + \mathbf{R}'\ (\langle C\rangle\mathbf{y_0})\mathbf{C}')$
$= R(\langle C\rangle) + R'\ (\langle C\rangle)\langle\mathbf{C}',\mathbf{v_0}\rangle + O(\varepsilon^2)$
$= R(\langle C\rangle) + O(\varepsilon^2)$.

Term 3: $(\mathbf{v_0})^T\ \mathbf{Q}_e(t)\mathbf{C}(t) = q_e(t)C_m(t)$
where, cup mixing concentration

$$C_m \equiv \frac{\mathbf{v_0}^T\mathbf{Q}_e\mathbf{C}}{\sum_{i=1}^N Q_i^{ex}} = \frac{\sum_{i=1}^N Q_i^{ex}C_i}{\sum_{i=1}^N Q_i^{ex}}$$

Term 4: $(\mathbf{v_0})^T\ \mathbf{Q}_{in}(t)\mathbf{C}_{in}(t) = q_{in}(t)C_{m,in}(t)$

where, $C_{m,in} \equiv \frac{\mathbf{v_0}^T\mathbf{Q}_{in}\mathbf{C}}{\sum_{i=1}^N Q_i^{in}} = \frac{\sum_{i=1}^N Q_i^{in}C_{i,in}}{\sum_{i=1}^N Q_i^{in}}$

Also $q_{in}(t) = \sum Q_i^{in}$ and $q_e(t) = \sum Q_i^{ex}$ is the total cumulative inlet and exit flow rates, respectively. Substituting above simplification in Eq. A12 we get

$$\frac{d}{dt}(V_R\langle C\rangle) + V_RR(\langle C\rangle) - q_{in}(t)C_{m,in}(t) + q_e(t)C_m = 0. \quad \text{(A13)}$$

The above equation relates bulk measurable quantities like cup-mixing and volume averaged concentration and total flow. For the case where $\|\boldsymbol{Q}(t)\| \gg 1$, i.e. very fast circulation, the concentration will be uniform and equal to $\langle C\rangle$. Thus for zeroth order, model equation reduces to

$$\frac{d}{dt}(V_{\mathrm{R}}\langle C\rangle) + V_{\mathrm{R}}R(\langle C\rangle) - q_{\mathrm{in}}(t)C_{\mathrm{m,in}}(t) + q_{\mathrm{e}}(t)\langle C\rangle = 0. \tag{A14}$$

Equation A13 can be solved to get temporal evolution of average concentration within the reactor provided there exist a closure relation, relating C_m and $\langle C\rangle$. To obtain that a local equation will be derived. Substitute Eq. A7 in Eq. A4 and keeping only leading order terms we get,

$$\mathbf{QC}' = \frac{d}{dt}(V_{\mathrm{R}}\boldsymbol{\alpha}\langle C\rangle)\mathbf{y}_0 + V_{\mathrm{R}}\boldsymbol{\alpha}R(\langle C\rangle)\mathbf{y_0} + \mathbf{Q}_e(t)\langle C\rangle\mathbf{y}_0 - \mathbf{Q}_{\mathrm{in}}(t)\mathbf{C}_{\mathrm{in}}(t). \tag{A15}$$

Now if we assume that although the total volume is function of time, volume fractions $\boldsymbol{\alpha}$ are constant, i.e., each cell is varying at constant rate. Then, we can rewrite Eq. A15 as

$$\mathbf{QC}' = \left[\frac{d}{dt}(V_{\mathrm{R}}\langle C\rangle) + V_{\mathrm{R}}R(\langle C\rangle)\right](\boldsymbol{\alpha}\mathbf{y_0}) + \mathbf{Q}_e(t)\langle C\rangle\mathbf{y}_0 - \mathbf{Q}_{\mathrm{in}}(t)\mathbf{C}_{\mathrm{in}}(t). \tag{A16}$$

Substituting Eq. A14 into Eq. A16 we get

$$\mathbf{QC}' = \left[q_{\mathrm{in}}(t)C_{\mathrm{m,in}}(t) - q_e(t)\langle C\rangle\right](\boldsymbol{\alpha}\mathbf{y_0}) + \mathbf{Q}_e(t)\langle C\rangle\mathbf{y}_0 - \mathbf{Q}_{\mathrm{in}}(t)\mathbf{C}_{\mathrm{in}}(t). \tag{A17}$$

Rearranging Eq. A17 we get,

$$\mathbf{C}' = \mathbf{inv}(\mathbf{Q})\left[q_{\mathrm{in}}(t)\boldsymbol{\alpha}\mathbf{y_0} - \frac{\mathbf{Q}_{\mathrm{in}}(t)\mathbf{C}_{\mathrm{in}}(t)}{C_{\mathrm{m,in}}(t)}\right]C_{\mathrm{m,in}}(t) - \mathbf{inv}(\mathbf{Q})\left[q_e(t)\boldsymbol{\alpha} - \mathbf{Q}_e(t)\right]\langle C\rangle\mathbf{y}_0. \tag{A18}$$

It may be noted that matrix $\mathbf{Q}$, having a zero eigenvalue, is not invertible. However, inverse can be defined using the constraint given by Eq. A11. From Eq. A7 $\mathrm{C_m}$ and $\langle C\rangle$ can be related by

$$C_{\mathrm{m}} = \frac{\mathbf{v_0}^T\mathbf{Q}_e\mathbf{C}}{q_e} = \frac{\langle \mathbf{C}\rangle\mathbf{v_0}^T\mathbf{Q}_e\mathbf{y_0} + \mathbf{v_0}^T\mathbf{Q}_e\mathbf{C}'}{q_e}, \tag{A19}$$

$$C_{\mathrm{m}} = \langle\mathbf{C}\rangle + \frac{\mathbf{v_0}^T\mathbf{Q}_e\mathbf{C}'}{q_e}. \tag{A20}$$

Substituting result obtained in Eq. A18 and after regularization we get

$$C_{\mathrm{m}} = \langle\mathbf{C}\rangle + \left(\frac{\mathbf{v_0}^T\mathbf{Q}_e}{q_e}\right)\mathbf{inv}(\mathbf{Q})\left[q_{in}(t)\boldsymbol{\alpha}\mathbf{y_0} - \frac{\mathbf{Q}_{in}(t)\mathbf{C}_{\mathrm{in}}(t)}{C_{m,in}(t)}\right]C_{m,in}(t) - \left(\frac{\mathbf{v_0}^T\mathbf{Q}_e}{q_e}\right)\mathbf{inv}(\mathbf{Q})\left[q_e(t)\boldsymbol{\alpha} - \mathbf{Q}_e(t)\right]\langle C\rangle\mathbf{y}_0, \tag{A21}$$

or

$$C_{\mathrm{m}} = \langle C\rangle + \tau_{\mathrm{mix,2}}C_{m,in} - \tau_{\mathrm{mix,1}}C_{\mathrm{m}}, \tag{A22}$$

where $\tau_{\mathrm{mix,1}}$ and $\tau_{\mathrm{mix,2}}$ are the dimensionless mixing times given by

$$\tau_{\mathrm{mix,2}} = \left(\frac{\mathbf{v_0}^T\mathbf{Q}_e}{q_e}\right)\mathbf{inv}(\mathbf{Q})\left[q_{\mathrm{in}}(t)\boldsymbol{\alpha}\mathbf{y_0} - \frac{\mathbf{Q}_{\mathrm{in}}(t)\mathbf{C}_{\mathrm{in}}(t)}{C_{\mathrm{m,in}}(t)}\right], \tag{A23}$$

and

$$\tau_{\mathrm{mix,1}} = \left(\frac{\mathbf{v_0}^T\mathbf{Q}_e}{q_e}\right)\mathbf{inv}(\mathbf{Q})[q_{\mathrm{e}}(t)\boldsymbol{\alpha} - \mathbf{Q}_{\mathrm{e}}(t)]\mathbf{y}_0, \tag{A24}$$

Equations A23 and A24 can be solved together with Eq. A13 to obtain temporal evolution of concentration within the reactor.

Intuitively, the dimensionless mixing times may be interpreted as the ratio of intake and exhaust flow rate to the circulation flow rate. As the in-cylinder circulation flow rate is much higher than the intake or exhaust flow rates, the dimensionless mixing times are usually in the range of $0 \le \tau_{\mathrm{mix,1}} \le 1$ and $0 \le |\tau_{\mathrm{mix,2}}| \le 1$. When both mixing times are zero, we have the ideal (perfectly mixed) model, while increasing magnitudes imply imperfect mixing. Now as the intake and exhaust flow rates vary with time, so will the mixing times. However, we use cycle averaged mixing times and assign a nominal value of 0.2 for $\tau_{\mathrm{mix,1}}$ and zero for $\tau_{\mathrm{mix,2}}$ (due to the assumption of pre-mixedness and no valve overlap). The model sensitivity to the first mixing time has also been reported.

Special cases: IC engine

1. Intake stroke: Assuming no valve overlap, during an intake stroke only intake valve is open, which implies $q_{\mathrm{e}} = 0$. Thus from Eq. A23–A24, we get $\tau_{\mathrm{mix,1}} = \tau_{\mathrm{mix,2}} = 0$
2. Compression and power stroke: During this period of engine cycle, both the valves are closed, there are no flow in or out of the system. Thus $q_e = 0$ and $\tau_{\mathrm{mix,1}} = \tau_{\mathrm{mix,2}} = 0$
3. Exhaust stroke: Only exhaust valve is open. As there is no inflow $\tau_{\mathrm{mix,2}} = 0$ but $\tau_{\mathrm{mix,1}} \neq 0$

For the case where valve overlap takes place, during the overlap period both the mixing times will be non zero.

Appendix B: Derivation of Energy Balance for In-Cylinder Combustion

From 1st law of thermodynamics,

$$\dot{Q} - \dot{W}_s + \sum_{j=1}^{N_c} F_j^{\mathrm{in}}H_j^{\mathrm{in}} - \sum_{j=1}^{N_c} F_jH_j = \frac{\partial\widehat{E}}{\partial t}, \tag{B1}$$

$$\widehat{E} = \sum_{j=1}^{N_c} N_jE_j,$$

Here N_j is the moles of jth component. The energy E_j is sum of internal energy U_j and the kinetic energy and the potential energy and the total energy is given by $\widehat{E}$. Neglecting changes in K.E and P.E we have,

$$\widehat{E} = \sum_{j=1}^{N_c} N_jE_j = \sum_{j=1}^{N_c} N_j(H_j - PV_j) = \sum_{j=1}^{N_c} N_j(H_j) - P\sum_{j=1}^{N_c} N_jV_j = \sum_{j=1}^{N_c} N_j(H_j) - PV_{\mathrm{R}} \tag{B2}$$

where H_j, V_j are the molar enthalpy and molar volume, respectively. Differentiating above equation w.r.t. time, we get

$$\frac{d\widehat{E}}{dt} = \sum_{j=1}^{N_c} N_j\left(\frac{dH_j}{dt}\right) + \sum_{j=1}^{N_c} H_j\left(\frac{dN_j}{dt}\right) - \frac{d}{dt}(N_{\text{Tot}}RT), \quad \text{(B3)}$$

where $N_{\text{Tot}} = \sum_{j=1}^{N_c} N_j$. Also from mass balance we have

$$\frac{dN_j}{dt} = F_j^{in} - F_j + \sum_{i=1}^{N_{\text{R}}} v_{ij}R_i(\langle C\rangle)V_{\text{R}}, \quad \text{(B4)}$$

substituting Eq. B4 in Eq. B3 we get,

$$\frac{d\widehat{E}}{dt} = \sum_{j=1}^{N_c} N_jCp_j\left(\frac{dT}{dt}\right) - \sum_{j=1}^{N_c} N_jR\frac{dT}{dt} - RT\sum_{j=1}^{N_c}\frac{dN_j}{dt} + \sum_{j=1}^{N_c} H_j\left(F_j^{\text{in}} - F_j + \sum_{i=1}^{N_{\text{R}}} v_{ij}R_i(\langle C\rangle)V_{\text{R}}\right), \quad \text{(B5)}$$

substituting above result in energy balance equation, we get

$$\dot{Q} - \dot{W}_S + \sum_{j=1}^{N_c} F_j^{\text{in}}H_j^{\text{in}} - \sum_{j=1}^{N_c} F_jH_j = \sum_{j=1}^{N_c} N_jCp_j\left(\frac{dT}{dt}\right) - \sum_{j=1}^{N_c} N_jR\frac{dT}{dt} - RT\sum_{j=1}^{N_c}\frac{dN_j}{dt} + \sum_{j=1}^{N_c} H_j\left(F_j^{\text{in}} - F_j + \sum_{i=1}^{N_{\text{R}}} v_{ij}R_i(\langle C\rangle)V_{\text{R}}\right), \quad \text{(B6)}$$

which simplifies to

$$\dot{Q} - \dot{W}_S + \sum_{j=1}^{N_c} F_j^{\text{in}}\left(H_j^{\text{in}} - H_j\right) - \sum_{i=1}^{N_{\text{R}}} R_i(\langle C\rangle)V_{\text{R}}\left(\Delta H_{\text{R},i}\right)_T + RT\sum_{j=1}^{N_c}\frac{dN_j}{dt} = \sum_{j=1}^{N_c} N_jCp_j\left(\frac{dT}{dt}\right) - \sum_{j=1}^{N_c} N_jR\frac{dT}{dt}, \quad \text{(B7)}$$

where $\left(\Delta H_{R,i}\right)_T = \sum_{j=1}^{N_c} v_{ij}H_j$. Assuming shaft work equal to work done by the piston $(P\dot{V}_R)$ we get,

$$\frac{dT}{dt} = \frac{1}{V_{\text{R}}\sum_{j=1}^{N_c}\langle C_j\rangle\left(C_{p_j} - R\right)} \times \left[\begin{array}{l} \dot{Q}_{\text{spark}} - \dot{Q}_{\text{coolant}} - P\dot{V}_{\text{R}} + \sum_{j=1}^{N_c} F_j^{\text{in}}\left(H_j^{\text{in}} - H_j\right) \\ +\left(\sum_{i=1}^{N_{\text{R}}} R_i(\langle C\rangle)V_{\text{R}}\left(-\Delta H_{\text{R},i}\right)_T\right) + RT\sum_{i=1}^{N_c}\frac{dN_j}{dt} \end{array}\right]. \quad \text{(B8)}$$

Above equation gives the temporal variation of temperature inside the combustion cylinder and is applied in Eq. 14.

Manuscript received Jun. 29, 2010, and revision received Sept. 16, 2010.